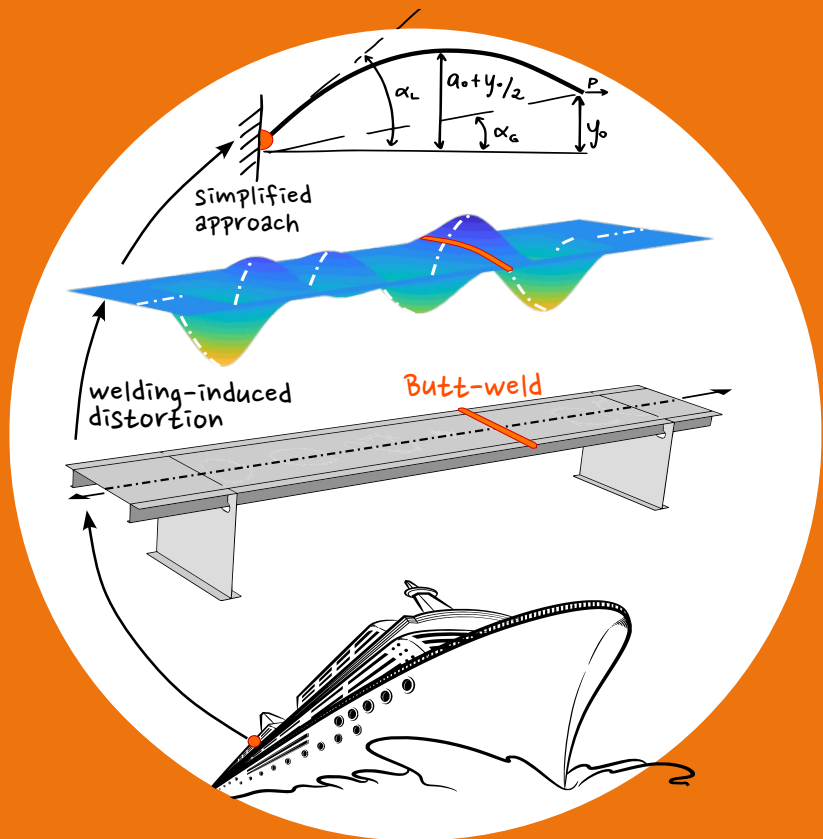


Enhancing the structural stress assessment of distorted lightweight ship deck structures

Federica Mancini



Enhancing the structural stress assessment of distorted lightweight ship deck structures

Federica Mancini

A doctoral thesis completed for the degree of Doctor of Science (Technology) to be defended, with the permission of the Aalto University School of Engineering, at a public examination held at the lecture hall 216/Otakaari 4 of the school on 13 June 2024 at 12:00.

Aalto University
School of Engineering
Department of Mechanical Engineering
Marine and Arctic Technology

Supervising professor

Professor Heikki Remes, Aalto University, Finland

Thesis advisor

Professor Jani Romanoff, Aalto University, Finland

Preliminary examiners

Doctor Inge Lotsberg, DNV GL, Norway

Professor Grzegorz Glinka, University of Waterloo, Canada

Opponent

Professor Grzegorz Glinka, University of Waterloo, Canada

Aalto University publication series

DOCTORAL THESES 123/2024

© 2024 Federica Mancini

ISBN 978-952-64-1868-1 (printed)

ISBN 978-952-64-1869-8 (pdf)

ISSN 1799-4934 (printed)

ISSN 1799-4942 (pdf)

<http://urn.fi/URN:ISBN:978-952-64-1869-8>

Unigrafia Oy

Helsinki 2024

Finland



Printed matter
4041-0619

Author

Federica Mancini

Name of the doctoral thesis

Enhancing the structural stress assessment of distorted lightweight ship deck structures

Publisher School of Engineering

Unit Department of Mechanical Engineering

Series Aalto University publication series DOCTORAL THESES 123/2024

Field of research Marine Technology

Manuscript submitted 8 March 2024

Date of the defence 13 June 2024

Permission for public defence granted (date) 20 May 2024

Language English

Monograph

Article thesis

Essay thesis

Abstract

Pursuing enhanced ship performance has driven lightweight structural solutions into modern cruise ship design. Among available strategies, the employment of thin steel plates in welded superstructure decks appears achievable, more sustainable and economically feasible. However, thin plates are susceptible to complex welding-induced distortions, which cannot be disregarded in the fatigue and limit state analysis of the welded structure. Since the effect of those distortions is not entirely considered by ship design rules, its evaluation requires full-field scanning of welded plates to be modelled in costly numerical analyses.

This thesis investigates computationally efficient structural stress assessment approaches on butt-welded 4 mm-thick plates in stiffened panels from actual shipyard production, resulting in average to severe initial distortions according to classifications in the marine structures community. The distortion measurement and characterisation are followed by the 3D geometrically non-linear finite element analysis (GNL-FEA) of the panels under tension, simulating the effect of hull girder bending on the superstructure decks. The 3D model is validated against uni-axial tensile tests on the panels. Thereafter, a gradual scale reduction from 3D to 2D and 1D models is performed numerically and analytically, where the von Kármán kinematic assumption accounts for the geometric non-linearity. As a last step, a beam model is developed for a simple half-sine curvature and considering the effect of weld rigidity.

In characterising the distortions, both amplitude and slope parameters need to be considered. For multi-buckled shapes with amplitudes below the plate thickness, a 2D analytical model neglecting the geometric discontinuity due to the weld can predict global structural stresses over the panel plate field; however, the weld cross-section must be considered in the local structural stress assessment of the welded area. For the latter, the 1D GNL-FEA of a distorted longitudinal profile located within 60% of the plate width results in less than 10% error. The 1D finite element model remains reliable if the distortion is included up to its first buckle from the weld location. Consequently, the analytical beam model can be adapted to the butt-welded area between thin plates in stiffened panels. Such an adaptation requires future research on the geometric parameters and boundary conditions in beam modelling.

Keywords Structural stress, thin plates, geometric non-linearity, computational modelling, lightweight design

ISBN (printed) 978-952-64-1868-1

ISBN (pdf) 978-952-64-1869-8

ISSN (printed) 1799-4934

ISSN (pdf) 1799-4942

Location of publisher Helsinki

Location of printing Helsinki **Year** 2024

Pages 160

urn <http://urn.fi/URN:ISBN:978-952-64-1869-8>

*To all readers, whether you stop at page four
or simply skim through the figures
of some crooked plates.*

Preface

My journey as a doctoral researcher in the Marine and Arctic Technology group of Aalto University began in November 2019. My doctoral research focused on analysing welding-induced distortions in thin plates, aiming at enhancing the structural stress assessment via time-efficient, simplified modelling approaches. The extensive body of research in fundamental theories of solid mechanics, as well as in ship structural design, has been instrumental in laying the foundation for my doctoral journey. Building upon such a foundation, the outcome of this thesis has addressed a research gap in the assessment of distorted thin plates, thus contributing to the development of engineering practices and future scientific breakthroughs in the design and assessment of thin-walled, large welded structures.

The doctoral studies were funded by the School of Engineering at Aalto University and the research projects RAMSSES (Realisation and Demonstration of Advanced Material Solutions for Sustainable and Efficient Ships) and CaNeLis (Carbon-neutral lightweight ship structures using advanced design, production, and life-cycle services). Their financial support and the grants received from the Merenkulun säätiö are greatly valued.

I am grateful to my supervisor, Professor Heikki Remes, and advisor, Professor Jani Romanoff, for their technical support, the opportunities provided, and the mutual trust built throughout the years. I also thank my research group, which has contributed greatly to my development and shared special moments along the way. I wish to thank Professor Emeritus Petri Varsta, who has never missed a chance to encourage me; and Professors J.N. Reddy and Arun Srinivasa, and their group at Texas A&M University, for the invaluable knowledge shared during my stay there.

I thank the pre-examiners, Doctor Inge Lotsberg and Professor Grzegorz Glinka, for their time, valuable opinions, and appreciation. Also, Professor Gary Marquis, as well as Doctors (and friends) Pasquale Gallo and Pauli Lehto, for proofreading and sharing helpful perspectives on the thesis.

In these years, I've cherished being surrounded by encouraging and inspiring people. Thank you, Meriam, Milad, Viktoria, Nadda, Bruno, *TheOfficeWomen*, *TheBigPictureThings*, and *BadJokesMasters* friends, the climbers, and the ELV scout group. Thank you, Tommaso, Miriam, Diana, and Arthur, for bringing such intense and genuine joy into my life. And thank you, Margherita and Nina, for your relentless support.

Before diving into the wonders of welding-induced distortions, I want to express my gratitude to my beloved mom and dad for the good care, education, and freedom they have provided for me. Grazie per esserci ed accogliermi sempre a braccia aperte.

Otaniemi, Espoo, May 15, 2024,

Federica Mancini

The reader should know that my love, Humberto, has dramatically affected my journey as a doctoral researcher. Perhaps, for good. Mesmo que não, sou grata a você por ser meu sol a cada dia.

Contents

Preface	3
Contents	5
List of Publications	7
Author's Contribution	9
Original features	11
List of Figures	13
List of Tables	17
Abbreviations	19
Symbols	21
1. Introduction	25
1.1 Background	25
1.1.1 Challenges in ship structural design	25
1.1.2 Lightweight design in cruise ships	27
1.1.3 Welding-induced distortions	29
1.1.4 Fatigue assessment of welded components with a distortion	31
1.1.5 Research gap	34
1.2 Scope of the thesis	34
1.2.1 Objectives	34
1.2.2 Limitations	36
1.3 Structure of the thesis	36
2. Methodology	37
2.1 3D scanning and modelling of distorted thin plates	38
2.2 Geometrically non-linear finite element analysis	39
2.2.1 Modelling of the welded area	39

2.2.2	3D finite element model	40
2.2.3	2D finite element model	41
2.2.4	1D finite element model	41
2.3	Analytical models	42
2.3.1	The radius of curvature	42
2.3.2	Von Kármán kinematics	43
2.3.3	2D plate theory	44
2.3.4	1D beam theory	46
2.4	Semi-analytical modelling of the weld rigidity	47
2.4.1	Computation of the fixity factors	48
3.	Results and Discussion	51
3.1	Geometry characterisation	51
3.2	From 3D FEA to 2D analytical solution	53
3.3	From 3D to 1D finite element analysis	56
3.4	1D analytical model	58
3.5	The influence of the weld profile	59
4.	General remarks and future work	61
4.1	Ideas for future research directions	67
5.	Conclusions	69
	References	71
	Errata	77
	Publications	79

List of Publications

This thesis consists of an overview and of the following publications which are referred to in the text by their Roman numerals.

I Mancini F., Remes H., Romanoff J., Lehto P., Rautiainen M., Niraula A., Niemelä A.. Shape characterisation and impact on the structural behaviour of initially distorted, 4-mm thick ship-deck stiffened panels. In *Marine and Offshore Structures, MARSTRUCT2023*, Sweden, 9, february 2023.

II Mancini F., Remes H., Romanoff J.. On the modelling of distorted thin-walled stiffened panels via a scale reduction approach for a simplified structural stress analysis. *Thin-Walled Structures*, 197,0263-8231, January 2024.

III Mancini F., Remes H., Romanoff J., Reinaldo Goncalves B.. Stress magnification factor for angular misalignment between plates with welding-induced curvature. *Welding in The World*, 64, 729-751, March 2020.

IV Mancini F., Remes H., Romanoff J.. A stress magnification factor for plates with welding-induced curvatures. In *Proceedings of the ASME 2020 39th International. Conference on Ocean, Offshore and Arctic Engineering, OMAE2020*, Virtual, August 2020.

V Mancini F., Remes H., Romanoff J., Gallo P.. Influence of weld rigidity on the non-linear structural response of beams with a curved distortion. *Engineering Structures*, August 2021.

Author's Contribution

Publication I: “Shape characterisation and impact on the structural behaviour of initially distorted, 4-mm thick ship-deck stiffened panels”

The author implemented the FE models of the stiffened panels using distortions from optical scanning measurements and performed the numerical analyses and validation based on the data from the monotonic tensile test of the panels. Furthermore, the author was responsible for preparing, editing, and revising the manuscript, as well as delivering the conference presentation.

Heikki Remes and Jani Romanoff supervised the work and contributed to the conceptualisation of the methodology, as well as to the editing of the manuscript.

Pauli Lehto collaborated in the experimental measurements that provided data presented in the study. Matti Rautiainen, Abinab Niraula, and Ari Niemelä were involved in the design, production and delivery of the panel specimens that were tested in the study.

Publication II: “On the modelling of distorted thin-walled stiffened panels via a scale reduction approach for a simplified structural stress analysis”

The author established the objectives and methodologies of the study. The author implemented the computational models, performed all the analyses and comparisons presented in the study, and was responsible for preparing, editing, and revising the manuscript.

Heikki Remes and Jani Romanoff supervised the work and contributed to the conceptualisation of the methodology, as well as to the editing of the manuscript.

Publication III: “Stress magnification factor for angular misalignment between plates with welding-induced curvature”

The author conceptualised, structured, and drafted the manuscript. The author derived and verified the analytical formulations, performed the sensitivity analysis detailed in the study, and edited and revised the manuscript.

Heikki Remes and Jani Romanoff supervised the work and contributed to the conceptualisation of the methodology, as well as to the editing of the manuscript.

Bruno Reinaldo Goncalves contributed to the manuscript writing and presentation of the results.

Publication IV: “A stress magnification factor for plates with welding-induced curvatures”

The author selected the methodology used in the study, formulated the analytical models, carried out the sensitivity analysis as presented in the paper, and was responsible for the manuscript preparation, editing, revision, and conference presentation.

Heikki Remes and Jani Romanoff supervised the work and contributed to the conceptualisation of the methodology, as well as to the editing of the manuscript.

Publication V: “Influence of weld rigidity on the non-linear structural response of beams with a curved distortion”

The author conceptualised the research. Accordingly, the author implemented the computational models, conducted all the analyses presented in the study, and was responsible for the manuscript preparation, editing and revision.

Heikki Remes and Jani Romanoff supervised the work and contributed to the conceptualisation of the methodology, as well as to the editing of the manuscript.

Pasquale Gallo contributed to the manuscript writing and presentation of the results.

Original Features

The design of lightweight cruise ship superstructures presents various challenges related to structural performance and optimisation. Scientific research has extensively covered aspects of thin-walled welded decks, with a particular focus on buckling and ultimate strength properties of plates with initial distortions. Similarly, substantial knowledge has been acquired regarding the fatigue performance of such structures, primarily from an experimental perspective.

It is evident that the initial distortion irregularity significantly influences the structural stress distribution over the panel plate field, leading to additional secondary bending actions on the plates, which, in turn, impact the fatigue life of the panels. Therefore, there is a need to adapt current computational tools and guidelines, particularly in the early stages of the ship design process.

In this context, the thesis assesses computational methods for evaluating the structural stress in welded thin plates with non-flat initial distortions. The objective is to streamline the structural stress analysis of thin-walled ship-deck stiffened panels. In light of this, the present work aims to contribute to the theoretical structural modelling of welded plates with an initial distortion and consider its practical implications in designing more economically and environmentally sustainable lightweight cruise ships.

The original features are listed below.

1. Distortion measurements and monotonic tensile test were conducted on 4 mm-thick ship-deck stiffened panels cut from a ship-deck demonstrator block [PI]. Comparing the experimental data to a shell element-based GNL-FEA (geometrically non-linear finite element analysis) of the panels reveals that the numerical predictions of structural stresses closely agree with the experimental results [PI]. The numerical simulations show that considering the actual shape of the distortion is necessary [PII], even if the axial and global angular misalignment are within the tolerances given by current design codes.

2. The response of stiffened panels with 2D complex initial distortions is assessed through GNL-FEA shell and beam element-based models and a plate theory based on the von Kármán kinematic assumption. The assessment shows the effects of welds, initial deformation shape (amplitude and slope), and its straightening under the action of uniform tension. Based on the analyses, simplified 2D and 1D models with more than 90% accuracy in terms of structural stress are proposed for the analysis of thin-walled stiffened panels [PII]. To the best of the author's knowledge, this kind of study aimed at an adequate scale reduction of the panel structural stress assessment has not been proposed before.
3. Geometric non-linearity is implemented in analytical models for the structural stress assessment by assuming small displacements and moderate rotations, i.e. von Kármán kinematics, which allows for including secondary bending terms. Accordingly, a second-order non-linear Euler-Bernoulli beam theory is proposed to model the mechanics of welded thin and slender non-stiffened plates with a simple curvature [PIII]. Based on the beam model, a novel stress magnification factor formulation was derived, which stands out for its conciseness and usability in structural engineering.
4. The beam model for a curved distortion is developed to include the weld rigidity as a non-ideal rotational constraint described by a fixity factor (ρ) in the weld location [PIV]. Based on common weld bead shapes for butt-welded thin plates available from the literature, the improved model is implemented in a semi-analytical procedure to evaluate the fixity factors. The study shows that typical weld beads correspond to ρ values between 0.9 and 1, thus being negligible in the case of very slender plates [PV].

List of Figures

1.1	Ship design spiral by J. Evans [1]	25
1.2	Structural levels of a cruise ship superstructure, transferring load and welding-induced initial distortions.	27
1.3	Typical panel distortions over the centre line [2, 3].	29
1.4	Hull-girder bending, hogging and sagging, causing membrane tension and compression on the panel unit.	30
1.5	Selection of structural stress-based approach for macro-geometry related imperfections among commonly accepted fatigue assessment methods. Modified from Radaj et al. [4].	31
1.6	Geometric parameters describing (<i>a</i>) axial and (<i>b</i>) angular misalignment between butt-welded plates, as in current IIW recommendations [5].	32
1.7	Geometric parameters describing the angular misalignment between butt-welded plates with a simple initial curvature. Modified from the IIW recommendations [5].	33
2.1	Top view of the panel model and related dimension parameters. The plate field (blue area) and the centre line (construction line) are indicated.	37
2.2	FE panel modelling procedure: from the distortion measurements and post-processing to the FE mesh via interpolation of three selected profiles.	39
2.3	Reduction in the modelling scale of the GNL-FEA of distortions of thin plates in stiffened panels.	40
2.4	FE model of the panel under uniform uni-axial tension. The weld detail shows the mesh refinement as recommended by the IIW for the structural stress extrapolation [5].	40

2.5	<i>a</i>) Longitudinal profile (blue line) at $Y_t = [50...175]$ mm-distance from the centre line at $Y = 0$; <i>b</i>) Profiles of the beam model, when spatial truncation of the distortion is performed over the X-direction at $\pm X_t$, symmetrically about the weld location in $X = 0$ mm.	42
2.6	Radius of curvature in the bending of a straight bar. Modified from Bazant et al. [6].	43
2.7	Simply-supported plate under uni-axial tension $N_{xx} = P$ over the x -direction.	45
2.8	Idealised beam model of a welded distorted thin plate under tension ($P > 0$).	46
2.9	Definition of the beam rotation angle (Φ_a) and the spring rotation angle (θ_a) at the left end (a) of the beam.	48
2.10	2D symmetric FE model of welded plates and a view cut near the weld region. The geometry and mesh distribution are shown, along with definitions and locations of interest for the present analysis.	49
3.1	Examples of (<i>a</i>) Contour plots for panel types P1 and P2, and (<i>b</i>) comparison of the panel centre line in ‘as-cut’ and ‘demo-block’ or ‘as-cut clamped’ configuration. Modified from [PII].	52
3.2	Comparison of the structural (S_{11}) to nominal (S_n) stress ratio in models <i>Panel</i> , <i>w-plate</i> , and <i>nw-plate</i> under 25 and 250 MPa. Empty and filled dots indicate peak stress centre line locations of top and bottom surfaces, respectively. . . .	54
3.3	Absolute error percentage for P1-type panels for loads of 25, 50, 150, and 250 MPa at the peak stress locations indicated in Fig. 3.2.	54
3.4	Comparison between measured distortions and analytical approximations along the Y direction. The absolute values of the measured data (black lines) are normalised with their maximum at relative peak amplitude locations (X_i) along the X direction; peak amplitude locations are indicated with blue dots in Fig. 3.1 <i>b</i>).	55
3.5	Error percentage plotted as a function of the absolute value of the maximum slope of the analytical solution compared to the numerical solution of a simply-supported, distorted plate under 150 MPa.	55
3.6	Maximum span to thickness ratio of the distorted configuration, $(w_1 + w_0)$, as a function of the nominal applied load for all panel specimens over their centre line.	56

3.7	Error percentage in the numerical stress estimation of the 1D beam model against the panel model <i>a</i>) within 10 mm (e_{10}) and <i>b</i>) 500 mm (e_{500}) from the weld location. Missing data beyond $e_{10,500} = 35\%$ are not shown.	56
3.8	Error percentage due to the beam translation over the plate width at $Y_t = [50\dots175]$ mm for panels P1.1 and P2.1 under 100, 150, and 250 MPa.	57
3.9	<i>a</i>) Stress comparison between panel model and beam with spatial truncation of the distortion at $X_t=400$ mm for panels P1.1; and <i>b</i>) maximum error percentage within 50 mm away from the weld of the beam with truncation at $X_t = [100,200,400]$ mm for all panels.	58
3.10	<i>a</i>) numerical (FEA) and analytical $k_{m,L}$ factor comparison, including the IIW formulation, $k_{m,G}$, for different angle ratios and both pinned, p , and fixed, f , BCs; <i>b</i>) percentage difference between the $k_{m,L}$ and $k_{m,G}$ as a function of the local-to-global angle ratio when $y_0 = 5$ mm and under fixed BCs.	58
3.11	Comparison between fixity factors (ρ_a) for different weld normalised areas ($area_N$) considering fixed rotational constraint at the end opposite to the weld location; see Table 2.3.	59
3.12	Stress magnification factor, k_m , as a function of the fixity factor, ρ_a , for different widths of the weld bead for SB and LB models with fixed rotational constraint at the end opposite to the weld. Δ_{max} is the maximum percentage difference between the k_m factor for $\rho_a = 1$ and the computed ρ_a	60
4.1	Simplified fatigue analysis for the estimation of the significant load range under long-term variable loading.	62
4.2	The use of modelling strategies for thin-walled stiffened panels with an initial distortion. Notes on the modelling of small-scale butt-welded specimens are also indicated, referring to analytical k_m formulations for local, L, and global, G, angular misalignment.	63
4.3	Misalignment definition in the adaptation of the analytical model in [PIII] to the panel distortions in Fig. 3.1	65
4.4	Percent difference between the numerical k_m factors from (<i>a</i>) stiffened panel models and (<i>b</i>) 1D numerical model of the panel distortion up to l_{hw} compared to the analytical $k_{m,L}$ and $k_{m,G}$ factors Table 4.2.	67

List of Tables

1.1	k_m factor formulations as DNV codes [7] and IIW recommendations [5], where $\alpha = 2y/l$ and $\beta = (2l/t)\sqrt{3\sigma_m/E}$	32
1.2	Thesis main topics and related publications.	35
2.1	Stress magnification factor (k_m) formulations from [PIII]. $C1$ and $C2$ coefficients are defined in Table 2.2.	47
2.2	$C1$ and $C2$ coefficients for the computation of the k_m factor using global (α_G) and local (α_L) angles.	47
2.3	Weld beads dimensions based on the idealised weld profile.	49
3.1	Right, $X_{w,r}$, and left, $X_{w,l}$, weld line coordinates, absolute maximum initial distortion, $ w_{0,max} $, and maximum span of the distortion profiles, Δw_0	52
4.1	Summary of the simplified modelling strategies proposed in the present work and their applicability for local and global structural stress assessment of the distorted plate field in stiffened panels.. . . .	64
4.2	Stress magnification factor formulations from IIW recommendations [5] and [PIII], considering fixed BC.	65
4.3	Misalignments measured for panels within the first half-wave on the right side of the welded joint; see Fig. 4.3 . . .	66

Abbreviations

BC	boundary condition
BV	Bureau Veritas
CPT	classical plate theory
db	demonstrator (or demo) block
DNV	Det Norske Veritas
EBT	Euler-Bernoulli beam theory
GNL-FEA	geometrically non-linear finite element analysis
HSS	high-strength steel
IACS	International Association of Classification Societies
IIW	International Institute of Welding
IMO	International Maritime Organization
ISO	International Organization for Standardization
LB	large bead
MB	medium bead
P1	panel with transverse butt-joint
P2	panel with transverse and longitudinal butt-joints
QE	quadratic extrapolation
RQ	research question
SB	small bead
T	topic
TTL	through-thickness linearisation
UHSS	ultra-high-strength steel
1D	one-dimensional
2D	two-dimensional
3D	three-dimensional

Symbols

a_{mn}	amplitude coefficient for trigonometric initial distortion with longitudinal, m , and transverse, n , wavelengths
a_0	amplitude of half-sine curvature
$area_N$	weld bead area normalised by the base plate area
A	cross-section area
b	width
b^*	constraint correction coefficient
b_{mn}	amplitude coefficient for trigonometric deflection with longitudinal, m , and transverse, n , wavelengths
b_p	plate width
B	stiffened panel width
D	total fatigue damage
D_p	plate flexural stiffness
e	axial misalignment between welded plates
e	error [%]
e_{10}	error at ± 10 mm distance from the weld location
e_{500}	error at ± 500 mm distance from the weld location
E	Young's modulus
E^*	effective Young's modulus
E_{ij}	Green-Lagrange strain tensor components
FAT	fatigue class (characteristic fatigue strength at $N = 2e10^6$)
G	shear modulus
h_w	weld toe/root height
I	second moment of inertia
k	Weibull shape parameter
$k_{a,b}$	rotational spring stiffness at beam ends a and b

k_m	stress magnification factor
$k_{m,ax}$	stress magnification factor due to axial misalignment
$k_{m,ang}$	stress magnification factor due to angular misalignment
$k_{m,G}$	stress magnification factor due to global angular misalignment
$k_{m,L}$	stress magnification factor due to local angular misalignment
l	length
l_{hw}	plate length up to the first half-wave
$l_{1,p}$	length of left plate in panel plate field
$l_{2,p}$	length of right plate in panel plate field
L	lengths between supports of welded plates
m	slope of the S-N curve
M_{ij}	bending moment
M_a	bending moment at beam end a
n	load cycles
N	number of cycles to failure
N_{ij}	axial force
w	final configuration including deflection and initial distortion
w'	first derivative of w (i.e., slope)
w''	second derivative of w (i.e., curvature)
w_{a_0}	initial half-sine curvature
w_{y_0}	initial lateral sway
w_0	initial distortion
$w_{0,max}$	maximum value of the initial distortion
$w_{0,min}$	minimum value of the initial distortion
w_1	deflection
W_{ext}	external work
w_w	weld width
p	probability density function
P	uni-axial load applied
$R_{a,b}$	rigidity coefficients
S_n	numerical nominal stress
S_{hs}	numerical structural hot-spot stress
S_{11}	numerical principal stress in x direction

t	thickness
$u_{(i,j,k)}$	displacement field components
U	numerical nodal axial displacement
UR	numerical nodal rotation
X_t	longitudinal coordinate of distortion truncation
$X_{(w,r/l)}$	right, r, and left, l, longitudinal coordinate of weld lines
y_0	amplitude of lateral sway
Y_t	location of distorted profile in the transverse direction
(x, y, z)	analytical coordinate system
(X, Y, Z)	numerical coordinate system
α_{a_0}	angular misalignment due to half-sine curvature
α_G	global angular misalignment
α_L	local angular misalignment
α_{y_0}	angular misalignment due to linear lateral sway
β	slenderness parameter
$\delta w_0 / \delta x_{max}$	maximum initial slope
Δ_{max}	maximum difference
Δ_{w_0}	maximum span of the initial distortion
ε_{ij}	analytical plate strain
ε^0	pure axial strain
ε^1	axial strain due to bending
$\phi_{a,b}$	beam rotation angle at ends a and b
$\Phi(x, y)$	potential energy density
γ_{xy}	analytical plate shear strain
λ	Weibull scale parameter
ν	Poisson coefficient
$\Pi(x, y)$	potential energy
ρ	radius of curvature
ρ_a	fixity factor at ends a and b
σ_m	membrane stress
σ_b	bending stress
σ_{hs}	analytical structural hot spot stress
σ_n	analytical nominal stress
σ_{ij}	analytical plate stress
σ_y	yield strength
$\theta_{a,b}$	spring rotation angle at beam ends a and b
θ_w	weld profile angle

well over a billion euros. Hence, cost and time optimisation is essential in each stage of the process.

In order to ensure the safety, reliability, and interoperability of ships, shipyards rely on the utilisation of standards, regulations, and guidelines such as DNV [8], IMO [9], ISO [10], and BV[11]. These documents are essential due to the complexity and diversity of design variables involved in shipbuilding. They guarantee compliance with environmental standards, cost-effectiveness, and high quality, and help ensure industrial best practices. The development of these design guidance documents is the result of extensive evaluation and collaboration between the scientific community and industry. Consequently, modernising the shipbuilding industry is a challenging and time-consuming process. Additionally, shipyards face the task of efficiently and cost-effectively implementing new design principles and construction techniques.

Despite such a conservative regulatory framework, over the last decades, there has been an emphasis on making shipbuilding more environmentally sustainable. The 2023 International Maritime Organization (IMO) GHG Strategy aims at a 40% reduction in the carbon intensity of international shipping by 2030 [9]. Therefore, improvement measures on operational efficiency and structural design are in the spotlight of the green transition in the maritime industry. According to the IMO, although not among the most polluting ones, the growing foreseeable cruise market calls for urgent actions by shipyards.

From a structural perspective, the design must comply with serviceability, ultimate, accident, and fatigue limit states to guarantee the functionality and safety of the structure. The limit states act as constraints in performing structural optimisation, which, in the pursuit of energy efficiency, means developing lightweight, strong and durable solutions.

Ships are large structures mostly composed of welded steel plates and beams. The characteristic modularity of the structure is built up by the repetition of a stiffened panel unit; see Fig. 1.2, showing the panel unit from the ship-deck block of a Cruise ship superstructure and their interactions. These panels consist of rigid sheets with a network of longitudinal and integrated transverse stiffeners. This construction ensures that the panels are robust and capable of withstanding the stresses of the marine environment.

The performance of the assembled structure is the result of multi-scale interactions, which makes the overall structural analysis very complex. Such complexity is typically handled by making strong simplifying assumptions in the computational models during the conceptual design phase and moving to gradually more comprehensive analyses towards the final stages. Typically, material and geometric imperfections in structural details are not included in full-ship models, but their stress-rising effect is considered via sub-modelling and partial safety factors. [5, 12, 13]

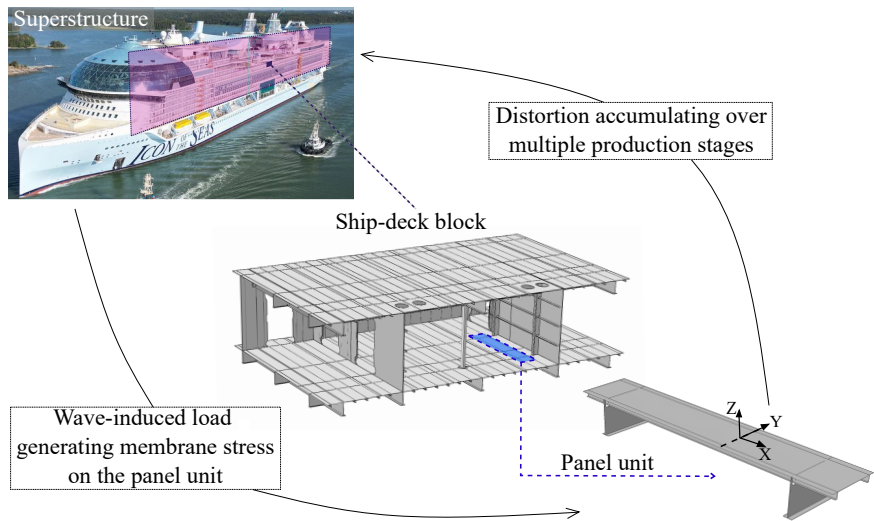


Figure 1.2. Structural levels of a cruise ship superstructure, transferring load and welding-induced initial distortions.

The structural assessment methods provided for the early design estimation of the partial safety factors (see, e.g., [5]) include calculations that generally avoid highly detailed and computationally costly numerical simulations. Guidelines propose simplified numerical models or analytical formulations that allow for closed-form solutions in the small-deformation field. These simplifications, however, restrict the design to acceptable dimensional ranges (e.g., thickness ranges) for the ship's components. Moreover, they do not apply to innovative structural arrangements. Therefore, in recent years, numerous research projects have focused on developing improved design and assessment methods for lightweight solutions in large ship structures, as explained in Section 1.1.2.

1.1.2 Lightweight design in cruise ships

Lightweight design concepts are utilised to optimize (in this case, minimize) the overall weight of the structure. Thinning, hollowing, and replacing materials are common lightweight strategies that have been extensively studied and implemented in the aerospace and automotive industries [14, 15], as well as considered in the marine technology field [16]. In the context of cruise shipbuilding, shipyards aim at a structural weight reduction by focusing on the ship superstructure, which houses the ship's accommodations, control centre, and other functional areas and amenities. These areas are compatible with a reorganisation of the spaces and allow for major innovation in the structural design. From a material point of view, structural steel is by far the most common construction material used in shipbuilding due to its high strength and ductile properties, which enable

the structure to withstand environmental overloads well beyond its elastic capacity. This would not be possible, for instance, with composite materials, the long-term performance of which is difficult to assess, thus currently remaining a non-viable option, despite their outstanding strength-to-weight ratio [17]. In terms of strength-to-weight ratio, aluminium, high-strength steel (HSS, with yield strength, σ_y , ranging between 300 and 550 MPa) and ultra-high-strength steel (UHSS, $\sigma_y > 550$ MPa) represent additional lightweight alternatives. Due to the stronger susceptibility of aluminium to welding defects such as hot cracking and porosity (see, e.g., [18]), and to similar defects detrimental to the fatigue performance of UHSS (see, e.g., [19]), the HSS has been the preferable option from a structural point of view. In addition, raw material and fabrication costs are cheaper because it can be used directly in production lines designed for normal structural steel including forming, welding, assembling, and painting. That is, there is no additional operating costs to update the shipyard facilities [20, 21].

From a topology perspective, innovative arrangements like sandwich panels have been studied in the context of large marine structures [22, 23, 24, 25]. However, these structures have poor fatigue strength (see, e.g., [26, 27]), and would require significant changes in the supply chain, as well as in the manufacturing facilities. Therefore, considering both implementation challenges and costs, the most straightforward action towards greener solutions for ship superstructures is the thinning of steel plates. Although requiring a different stiffener spacing, it allows for preserving a modular configuration of the superstructure, using thin-walled stiffened panels as a basic modular unit.

An example was presented by Lillemäe et al. [12], where 3-mm thick steel plates were used in the upper decks of a superstructure with a traditional design. A 43% reduction in weight per deck was reported, which meant a significantly lighter structure. Although the load-carrying capacity of the thin decks was reduced, the overall load-carrying capacity of the structure did not significantly change, since these decks do not comprise a main load-bearing part of the ship. Therefore, the authors showed that the thinning of the upper deck is a viable and valuable strategy in this context.

However, thin plates cause different vibratory responses, proneness to instability, and higher sensitivity to the onset of manufacturing-induced imperfections that affect the characteristic limit states of the structure. Imperfections can be weld cracks, porosity, incomplete penetration, lack of fusion, undercut, imperfect weld profile and distortions. In the development of thin-walled ship superstructures, particular attention is needed on welding-induced distortions, which generally become more irregular, thus challenging the understanding of the mechanical response of the welded structures.

1.1.3 Welding-induced distortions

The formation of welding-induced distortions depends on a combination of factors including the welding process and the properties of the materials being joined [28, 29, 30]. Welding implies a heating-cooling cycle of the materials that results in expansion followed by contraction. As the molten weld metal solidifies, it eventually contracts. In addition to metallurgical changes, this contraction causes the component to deform and experience residual stresses based on the constraint used in the production. This constraint varies across production phases, being well-defined during panel production and becoming increasingly uncertain towards ship assembly.

Pre-stressing the components in the opposite direction of expected distortions, using low-heat input welding processes like laser-hybrid welding [31], and post-weld heat treatments can all help minimise the distortions. Nevertheless, welded plates never remain ideally straight [32, 33]; see Fig. 1.3, which shows typical distortions commonly known as ‘hungry horse’, ‘mountain mode’, ‘spoon mode’, ‘sinusoidal mode’, and ‘buckling mode’ observed over the centre line of welded plates in stiffened panels [2].

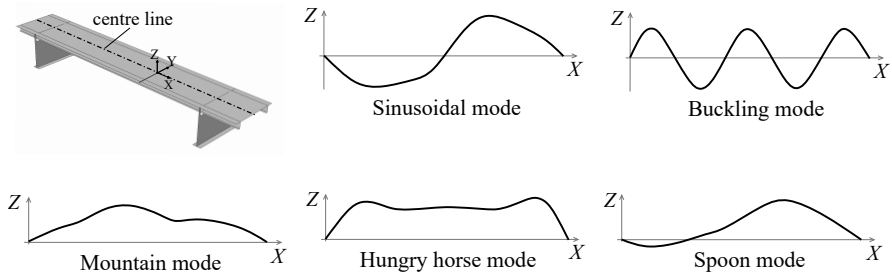


Figure 1.3. Typical panel distortions over the centre line [2, 3].

Comprehensive research has demonstrated the non-negligible effect of initial distortions on the mechanical response of plates, which can affect the performance of the entire structure [34, 35]. The distortions cause non-linear secondary bending moments and, thus, additional stress concentrations on plates subject to membrane forces. Such forces act on the panel units due to the hull-girder global bending, as shown in Fig. 1.4 [36]. The buckling and ultimate strength properties of stiffened panels with an initial distortion have been considered in several studies [34, 35, 37, 38, 39, 40, 41], where load-end-shortening curves of the component under compression reveal changes in its global stiffness. In this context, well-known simplified closed-form analytical solutions (see, e.g., [42]) have been a starting point to develop more sophisticated solutions for combined loads and complex framing arrangements [43, 44, 45, 46, 47, 48]. In principle, the distortion is approximated by an ideal trigonometric series able to reproduce the typical distortions shown in Fig. 1.3.

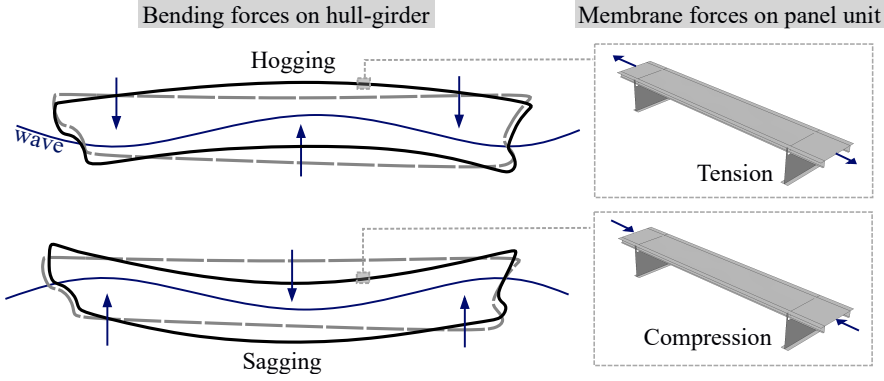


Figure 1.4. Hull-girder bending, hogging and sagging, causing membrane tension and compression on the panel unit.

Based on buckling and ultimate strength analyses of distorted plates, guidelines and regulations for the classification and tolerance limits of the initial distortion in large welded structures have been defined [36, 49]. Accordingly, the severity of distortion is determined by a plate slenderness parameter, defined as $\beta = (b/t)\sqrt{\sigma_y/E}$, where b and t are the plate width and thickness, respectively, σ_y is the yield strength of the material, and E its Young's modulus. This term indicates sturdy plates when $\beta < 2.4$ and slender plates for $\beta > 2.4$. For thin and slender plates, the level of severity is expressed by the maximum amplitude of the initial distortion, $w_{0,max}$, as in Eq. 1.1 [36].

$$w_{0,max} = C_2 \beta t, \quad \text{where:} \quad C_2 = \begin{cases} 0.025 & \text{slight level} \\ 0.1 & \text{average level} \\ 0.3 & \text{severe level} \end{cases} \quad (1.1)$$

By contrast, the IACS guidelines allow for up to $w_{0,max} = 6\text{-}9$ mm for distorted plates in stiffened panels [49]. Over the mentioned tolerance limits, large deflection theories are recommended for the analysis of the structures. Hence, simplified solutions lose their validity and numerical analysis often becomes indispensable. Nevertheless, the limited research available on the characterisation of measured welding-induced distortions on thin plates in stiffened panels (see, e.g., [33, 50]) suggests that the distorted shapes can be visibly irregular and present a curvature near the weld. This may affect the mentioned tolerance limits, thus requiring further research on the distortion shapes and their effect on the mechanics of thin plates.

In addition to ultimate strength analyses, given a life expectancy exceeding 20 years and the characteristic cyclic loads of the marine environment, investigating the detrimental impact of the distortions on the fatigue performance of ships is also of fundamental importance [31]. For this reason, there is a need to better define the local response of the panel at the regions

of stress localisation (i.e., hot spots) where assessment is more sensitive to the accuracy of the shape approximations. This has led to further research in the development of analysis methods and simplified solutions, which are yet to be established. In Section 1.1.4, the treatment of geometric imperfections in the fatigue strength assessment of welded structures is discussed more in detail.

1.1.4 Fatigue assessment of welded components with a distortion

Fatigue strength assessment evaluates the potential for fatigue failure in materials and structures undergoing repetitive and cyclic loading, such as wave-induced loads on cruise ship hull girders [51]. Such a failure typically follows from the initiation and growth of cracks due to the presence of material, micro-, and macro-geometric defects (e.g., inclusions, surface roughness, notches, etc.).

The fatigue performance of a structure can be assessed via several methods, which are suitable for different applications [4, 52]. A summary of the well-known methods is given in Fig. 1.5.

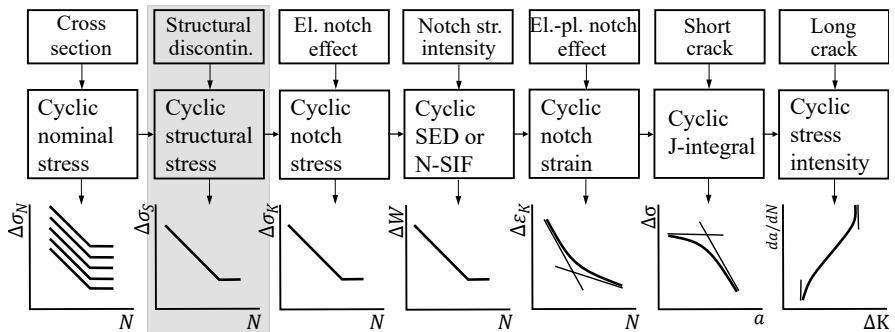


Figure 1.5. Selection of structural stress-based approach for macro-geometry related imperfections among commonly accepted fatigue assessment methods. Modified from Radaj et al. [4].

The effect of macro-geometric distortion can be estimated via a local stress-based method [53] such as the structural hot-spot stress approach which estimates the stress concentrations due to geometric effects in locations where fatigue damage is expected [5, 7]. Especially for the early design phase, the stress concentrations are quantified by an analytical stress magnification factor, k_m . The factor is defined by the ratio between the structural and the applied nominal stress, and it is calculated based on the contribution of an *axial* e and *angular* α misalignment, as in Eq. 1.2 [5, 7]. The axial misalignment refers to the relative offset between plates, while the angular misalignment to the angle generated by a linear lateral sway of amplitude y_0 , thus describing a linear geometry, i.e., a flat beam;

see Fig. 1.6.

$$k_m = 1 + (k_{m,ax} - 1) + (k_{m,ang} - 1) \quad (1.2)$$

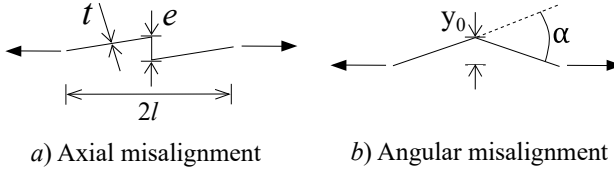


Figure 1.6. Geometric parameters describing (a) axial and (b) angular misalignment between butt-welded plates, as in current IIW recommendations [5].

Considering the ship design codes (e.g., DNV [7]), the k_m factor formulations are developed for flat plates under pinned and fixed boundary conditions (BCs) on an Euler-Bernoulli beam model with a flat initial distortion; see Table 1.1, where l and t are the component length and thickness, respectively, σ_m is the applied membrane stress, and E describes the Young's modulus for a linear-elastic material. In the Table, the formulations from the International Institute of Welding (IIW, [5]) are also presented. Those are considered to be the reference k_m formulations for the present work, as they represent an evolution of the formulations in [7] towards considering the straightening effect¹ of the angular misalignment under tensile load. Also based on the Euler-Bernoulli Theory, they consider the developing deformation in computing a secondary bending moment that follows the non-linear interaction between load and distortion. In the context of beam theories, this has been denoted as second-order beam theory, where the von Kármán kinematics is assumed to consider the secondary bending moments (see, e.g., [42]); more is explained in Section 2.3.2.

Table 1.1. k_m factor formulations as DNV codes [7] and IIW recommendations [5], where $\alpha = 2y_0/l$ and $\beta = (2l/t)\sqrt{3\sigma_m/E}$.

	Pinned BC	Fixed BC
[7, 5]	$k_{m,ax} = 1 + \frac{3e}{t}$	$k_{m,ax} = 1 + \frac{3e}{2t}$
[7]	$k_{m,ang} = 1 + \frac{3\alpha l}{t}$	$k_{m,ang} = 1 + \frac{3\alpha l}{2t}$
[5]	$k_{m,ang} = 1 + \frac{3\alpha l}{t} \frac{\tanh(\beta)}{\beta}$	$k_{m,ang} = 1 + \frac{3\alpha l}{2t} \frac{\tanh(\frac{\beta}{2})}{\frac{\beta}{2}}$

The current IIW k_m factor formulations were initially presented to the IIW by Kuriyama et al. [54] and later adapted to different butt-joint configurations by Maddox [55]. They are largely used in the fatigue assessment of welded structures presenting misalignment. However, in deriving these formulas, it was assumed that the plates remain geometrically flat in the vicinity of the weld.

¹Reduction of the out-of-plane distortion along the direction of a tensile load.

Based on the experimental observations by Eggert et al. [33] and Lillemäe et al. [50], the distorted shape in the welded area cannot be considered flat, and thus the formulations in Table 1.1 cannot be considered adequate for thin plates [50, 56]. In this regard, stress magnification factors for the fatigue assessment of distorted thin plate specimens for simple initial curvatures, as in Fig. 1.7, have been recently proposed [57, 58, 59].

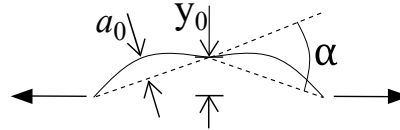


Figure 1.7. Geometric parameters describing the angular misalignment between butt-welded plates with a simple initial curvature. Modified from the IIW recommendations [5].

The solutions presented by Zhou et al. [57] and Shen et al. [59] have high originality and contribute to the development of the structural stress-based fatigue assessment of thin-walled welded structures, although their studies have not converged to an established analytical modelling approach for distorted thin plates. On one hand, Zhou et al. [57] modelled the curved distortion as a lateral dummy load able to describe the effect due to a variety of shapes, yet providing a relatively complex solution compared to the ones in Table 1.1. On the other hand, Shen et al. [59] considered the distortion in terms of a secondary bending moment using a parabolic shape. By comparison, the second case results in a more concise solution, which however uses a polynomial approximation of the curvature, thus being limited to simple shapes due to the fast increase in order in the approximation series when complex realistic distortion shapes are considered². Therefore, further research is needed towards developing k_m factor formulations for a sufficiently accurate and efficient structural hot-spot stress fatigue assessment of welded thin plates.

Furthermore, these stress magnification factor solutions have been verified against numerical models of small-scale specimens. However, their validity for distorted full-scale thin plates in stiffened panels has not been demonstrated. In such a case, the stiffening frame and the 2D development of more complex distortion lead to an in-plane redistribution of the stresses that also affects the consequent behaviour of the plates [33, 50].

²Unlike trigonometric series, polynomial ones require a balance between shape and order for approximating complex distortions. They lack periodicity, resulting in extrapolation issues and divergent solutions beyond the data range.

1.1.5 Research gap

Especially in the case of complex initial distortions, previous research has focused on the analysis of thin-plated stiffened panels relying on the Geometrically Non-linear Finite Element Analysis (GNL-FEA) [50, 56, 60]. Although accurate, this approach is computationally inefficient when applied to the design of large structures such as ships, comprising hundreds of repeating units [13]. This explains the efficacy of highly simplified analytical and numerical models or experimental benchmarks for the evaluation of geometric stress concentrations, as given in design standards. However, current standards apply to relatively thick plates. As a consequence, shipbuilding design codes indicate a minimum allowed thickness of 5 mm for deck plates; see, e.g., [7].

Nevertheless, the studies conducted by Lillemäe et al. [50] and Fricke and Feltz [60] demonstrated that thin-walled panels show sufficient fatigue strength based on the design S-N curves provided by the IIW recommendations, despite the measured lateral distortion and axial misalignment values exceed the current tolerance limits by 35% and 50%, respectively [33]. The assessment considered tolerances given in several guidelines relevant to shipbuilding [61]. This confirms that the existing design guidance documents do not adequately reflect the mechanical behaviour of thin plates. Therefore, it is relevant to evaluate the feasibility of extending these design guidance documents to the assessment of moderately deformed structures, as required for developing innovative lightweight solutions.

The development of models that can explicitly consider the real geometry of the welded plates is also a way to avoid the use of estimated stress concentration factors based on the average expected fabrication quality. Although the advances in manufacturing technologies allow for improved quality, i.e., less critical stress concentrations on the structures, the assumed fabrication tolerances are not always met by all shipyards worldwide. This challenges the accepted practice of embedding the effects of imperfections in safety factors, especially for the fatigue life assessment and the estimation of life-cycle maintenance costs [62].

1.2 Scope of the thesis

1.2.1 Objectives

In light of the above, with the growing interest in the development of lightweight cruise ship superstructures, new challenges have arisen due to the onset of complex welding-induced distortions on thin plates that

generate non-negligible geometric non-linear stress-rising effects. In this regard, extensive research has demonstrated the inadequacy of available engineering design tools for the fatigue assessment of these structures.

The research question that the present thesis aims to answer is: *when and how does the complex geometry of an initially-distorted welded plate need to be considered for an efficient structural stress assessment of large welded lightweight structures?*

This thesis focuses on the characterisation of welding-induced distortions on thin plates and their effect on the behaviour of thin-walled stiffened panels. The aim is to propose computationally efficient strategies for the structural stress assessment of such structural components. In this context, plates are less than 5 mm thick and slender, i.e., $L/t > 20$, with L as the length between two supports.

The study considers real and relatively complex distortions measured on 4-mm full-scale stiffened panels. The panels are part of a demonstrator block of a ship superstructure deck. The monotonic tensile test of these panels is used to validate the 3D finite shell element-based model under geometrically non-linear analysis. Then, a gradual reduction to 2D and 1D modelling scales is proposed, also considering existing plate and beam theories. The study is conducted with a major interest in the estimation of structural stresses of the plates under uni-axial tension.

The publications that are appended as part of this thesis address the following three topics (T):

- T1: Simplifying the modelling of distorted stiffened panels under tension for structural stress assessment.
- T2: Exploring the feasibility of developing a concise analytical formulation for the structural hot-spot stress for butt-welded thin and slender plates under uni-axial load.
- T3: Consideration of the combined effect of weld geometry and welding-induced distortion on the structural hot spot stress estimation.

The reader can find specific information on the research topics by consulting the scientific articles based on Table 1.2.

Table 1.2. Thesis main topics and related publications.

	PI	PII	PIII	PIV	PV
T1	x	x			
T2		x	x		
T3				x	x

1.2.2 Limitations

The effect of the macro-geometry on the stress distribution around the welded area is independent of other stress concentrations [63]. For this reason, the influence of additional stress-rising effects is not considered in the study.

When modelling the transversely butt-welded thin plates in stiffened panels, the study makes use of solid mechanic theories of beams and plates under plane stress conditions and in the range of small elastic deformations, including moderate rotations of the components under uniaxial tension. Such a range is justified by the focus on load levels typical for the high-cycle fatigue regime. Tension is the only loading mode considered due to its crack-opening effect and primary contribution to fatigue damage of the structure. In addition, tension is the primary loading acting on superstructure decks in passenger ships. This is due to still water bending moments from a concentration of buoyancy force at midship area, leading to hogging conditions while redistributing the ship weight more uniformly [64]. Accordingly, this study does not explicitly consider mean stresses, which implicitly add to the nominal applied tension.

While the study lies within the context of structural fatigue, the primary interest is in developing simplified computational methods for the structural hot-spot stress assessment of the welded components. Therefore, the thesis does not focus on fatigue strength and damage calculations, which are largely present in the literature [33, 50, 65, 66, 67].

Focusing on the mechanics of existing distortions, different welding techniques or post-welding treatments are not discussed. Therefore, the study targets distortions that are not sufficiently large so as to require, e.g., expensive straightening treatment or mass-evening techniques, which do not align with an economically sustainable lightweight design principle.

Furthermore, the findings from this study cannot be extended to arbitrary panel dimensions without proper investigation of the type of initial distortions that are likely to form during manufacturing. This is because, although the computational models can be adapted to different geometries, the conclusions drawn in the current work are based on a limited dataset of geometry measurements.

1.3 Structure of the thesis

The thesis will present the theoretical framework and methods of the study in Chapter 2. The main results are presented and discussed in Chapter 3, which is followed by a general discussion and the final remarks in Chapters 4 and 5, respectively. The scientific publications related to this work are appended to the thesis.

2. Methodology

This chapter summarises the approaches used in modelling and analysing the mechanics of distorted butt-welded plates. The study is based on real distortions measured on a ship block as shown in Fig. 1.2. Unlike previous investigations on full-scale panel structures [33, 68, 56], the opportunity to investigate panel units from a real block of a ship deck allowed the study to observe distortions produced by the actual welding sequence and boundary conditions in shipyard procedures. Later assembling in the hull erection phase will change the distortions only locally, near the block boundaries, meaning that the block well represents the final distortion shapes of the majority of the panel units.

Figure 2.1 shows a top view of a typical panel unit herein considered, indicating the relevant geometric parameters describing the panel and its plate field, i.e., the blue area in Fig. 2.1. In developing simplified modelling

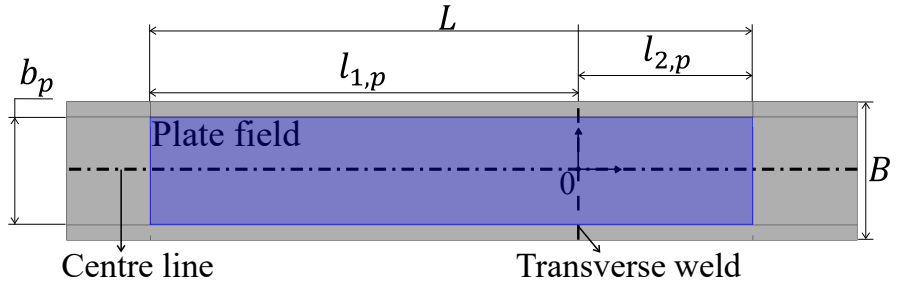


Figure 2.1. Top view of the panel model and related dimension parameters. The plate field (blue area) and the centre line (construction line) are indicated.

approaches, the effects of the stiffening frame and the weld geometry are addressed. Numerical 3D, 2D, and 1D models, as well as 2D plate and 1D beam analytical models, are implemented for the structural stress assessment of welded components. The beam model is then extended to non-ideal rotational constraints representing the presence of a non-ideally rigid weld seam between the plates.

It is also noticeable that due to inaccuracies of in-situ measurements, the scans of the panels before cutting were incomplete, therefore the

study on the modelling simplifications refers to the distortions measured after the panels were cut from the demo block. In addition, although the panel unit isolated from the surrounding structure may not fully represent the in-service response of these units, it was not feasible to conduct experimental research on larger and more complex structural blocks due to practical limitations in the testing facility. For these reasons, the distortions considered in the thesis may not represent the full range of distortions found on ship superstructures. Nonetheless, the application of the developed modelling approaches is meant to go beyond the case studies available in this work.

2.1 3D scanning and modelling of distorted thin plates

Welding-induced distortions have typically been classified in terms of axial and angular misalignment between welded plates, as shown in Fig. 1.6 [5]. In the case of flat distortions, typically observed on plates thicker than 5 mm, both quantities can be measured to an adequate degree of accuracy by utilising dial gauges [62]. However, there are no generally accepted protocols to define an angular misalignment in the presence of local curvatures. For this reason, the geometry characterisation of irregular distortions requires the definition of more parameters based on a comprehensive analysis of the distortion over the entire plate field. Therefore, having access to optical laser full-field scanning instruments is a great advantage in terms of time and accuracy for high-precision images over extended surfaces.

In this study, distortions were measured using ATOS Compact Scan 12MP optical measurement system provided by GOM GmbH [69]. The system consists of two 12-megapixel stereo cameras with a measurement resolution of 0.126 mm based on a measuring volume of $1200 \times 900 \times 880$ mm³. It operates by projecting a series of structured light patterns onto the scanned surface. Such patterns are deformed according to the surface geometry, and their deformations and positions are used by the GOM Inspect software to reconstruct the 3D shape of the object. The software is used for the polygonisation of the scans to be further post-processed and analysed using Matlab. Cubic interpolation is used to generate a regular 4-noded rectangular mesh from three longitudinal profiles extracted from the scans at $Y = [-120, -5, 120]$ mm within the transverse frames located at $X = [-1740, 818.5]$ mm; see Fig. 2.2. This was determined as the minimum sufficient number of profiles for a reliable representation of the distortion over the plate field [PI]. The left and right ends of the generated mesh are aligned to $Z = 0$ mm.

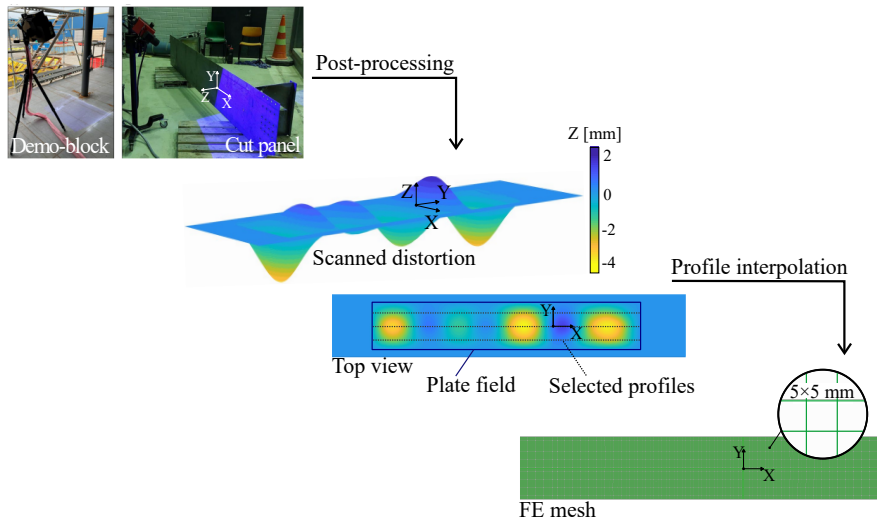


Figure 2.2. FE panel modelling procedure: from the distortion measurements and post-processing to the FE mesh via interpolation of three selected profiles.

2.2 Geometrically non-linear finite element analysis

The FE model of the panel was generated by assembling the orphan mesh of the distorted plate field with an ideally straight stiffening frame. Any simplification of such a model was performed maintaining the plate field distortion realised from the experimental measurements.

The models were created using Python-Abaqus scripting [70], and the Abaqus static solver was used for the static GNL-FEA of the models under uniform tension. The post-processing of the numerical results was carried out in Matlab.

In all the simulations, the material is a common structural steel, with a Young's Modulus of $E = 209$ GPa and Poisson's ratio of $\nu = 0.3$. All the analyses presented in this thesis remain in the linear-elastic range of the material, as only small-scale yielding at the notch tip exists in the load level typical for the high-cycle fatigue regime considered in this work.

The next sections describe the modelling of the weld, followed by the reduction in modelling scale from a 3D shell element-based model, through a 2D model, and to a 1D model. An overview of the models is given in Fig. 2.3.

2.2.1 Modelling of the welded area

The weld profile is idealised into a rectangular cross-section. Based on the geometry measurements, the weld thickness is equal to 6 mm, i.e., 2 mm larger than the plates; see Fig. 2.4. The width of the cross-section varied between 3 and 5 mm, based on the specific panel under considera-

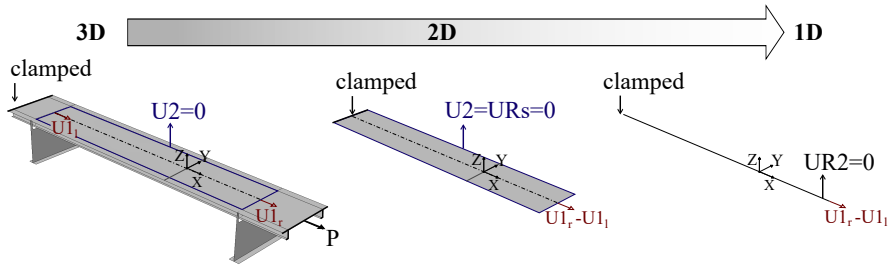


Figure 2.3. Reduction in the modelling scale of the GNL-FEA of distortions of thin plates in stiffened panels.

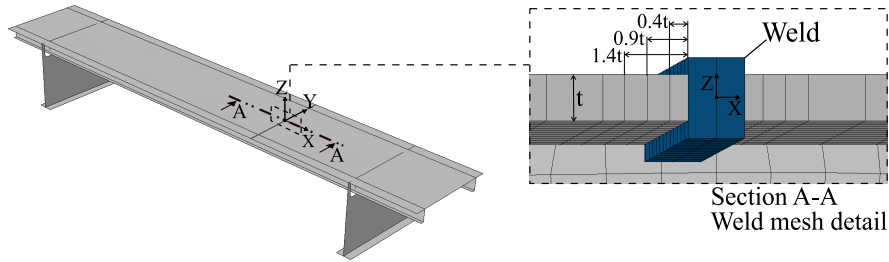


Figure 2.4. FE model of the panel under uniform uni-axial tension. The weld detail shows the mesh refinement as recommended by the IIW for the structural stress extrapolation [5].

tion. The IIW provides guidelines for the geometry simplification needed when assessing structural hot-spot stress. In addition, a refined mesh is recommended for extrapolating structural stress within a short distance, i.e., $[0.4, 0.9, 1.4]t$ mm, from the weld lines, as depicted in Fig. 2.4.

2.2.2 3D finite element model

The 3D FE panel model, including butt-welded plates and stiffening frame, presents a mesh with square 4-noded shell-elements of 5 mm with reduced integration and hourglass control, indicated as S4R elements in Abaqus FE package library. The assembly comprises tie constraints between adjacent parts. A concentrated uni-axial tension, P , is applied uniformly on the right edge of the panel through a coupling constraint between the edge and the reference point of application. The panel's left edge is fully clamped, while the other edges are free to slide in the X direction. The reliability of the GNL-FEA of the panel model is based on the experimental validation of the model with free lateral edges. Such validation is conducted through the monotonic tensile test of the panels shown in Fig. 2.1. The strains at a 5-mm distance from the butt-weld lines on both top and bottom surfaces from the numerical analysis resulted in a maximum error of 13% compared to the experimental results, mainly due to possible inaccuracies in the placement and orientation of the strain gauges. More details on the

validation can be found in [PI]. In this work, the panel model provides a reference solution to evaluate the simplified 2D and 1D models, which are presented next.

2.2.3 2D finite element model

Compared to the 3D model described above, the 2D one does not include the stiffening frame, which is replaced by ideally rigid rotational constraints, URs, over the plate edges.

An equivalent loading condition is obtained by imposing a uniform axial displacement to the right edge of the plate equal to the one of the panel. Such displacement is computed as the difference between the displacement U_1 at the transverse frames, i.e., $(U_{1r} - U_{1l})$ as shown in Fig. 2.3. Imposing an axial displacement is consistent with a sub-modelling approach used in ship design, where local structural components are typically considered under displacement control [13].

Such a model is used as a transition from the panel model to its 1D representation described in Section 2.2.4. Moreover, the plate simulations are needed as a verification of the plate analytical models presented later in Section 2.3.3.

2.2.4 1D finite element model

The 1D model reduces the plate field into a beam, which only represents a distortion profile in the longitudinal direction. In representing a plate field, a beam model is typically modified to account for the Poisson's effect¹ with effective Young's modulus $E^* = \frac{E}{1-\nu^2}$. Nevertheless, in this study, an equivalent strain and stress field between the panel model and the beam is ensured by imposing the axial displacement of the panel on the beam model, as explained for the 2D model; see Fig. 2.3.

The beam element-based model is initially used to represent the panel centre line. Next, to understand the flexibility of using such a model, its accuracy is studied by considering a translation across the plate width and a spatial truncation of the distortion along the beam length.

Beam translation over the plate width - To understand the influence of the rotational constraints on the plate lateral edges, the beam model is translated over the plate width to predict the stress distribution over the distortion profiles on the sides of the centre line. This translation can be beneficial in the case of distortions asymmetric to the centre line. Analyses are conducted for distortion profiles at $Y_t = [50, 100, 150, 175]$ mm

¹Lateral contraction or expansion of a structure under uni-axial tension and compression, respectively. The Poisson's coefficient, ν , is defined as the transverse-to-longitudinal strain ratio.

from the weld centre line; see Fig. 2.5(a).

Spatial truncation of the distortion - A truncation of the distorted profile over its length is performed to find the minimum spatial observation window for a sufficiently accurate structural hot-spot stress assessment. Truncations occur at $X_t = \pm[100, 400]$ mm from the weld, as shown in Fig. 2.5(b).

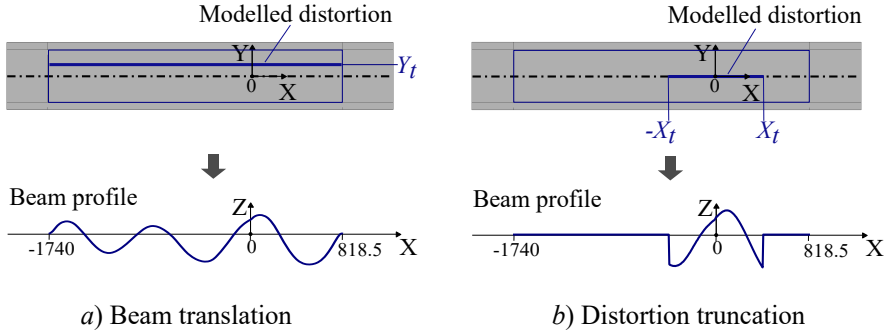


Figure 2.5. a) Longitudinal profile (blue line) at $Y_t = [50...175]$ mm-distance from the centre line at $Y = 0$; b) Profiles of the beam model, when spatial truncation of the distortion is performed over the X -direction at $\pm X_t$, symmetrically about the weld location in $X = 0$ mm.

2.3 Analytical models

Plate theories model the 3D solid continuum as a two-dimensional (2D) model when the in-plane dimensions are significantly larger than the thickness dimension. This is the case for the welded plates in the stiffened panels. Moreover, when the plate length is considerably larger than the width, the plate can be considered as a plate strip, which behaves like a beam under certain conditions. Therefore, both plate and beam theories are considered in the context of this study. This section introduces a plate and a beam analytical model based on classical theories with a linearised radius of curvature which is then extended to include moderate rotations by assuming von Kármán kinematics.

2.3.1 The radius of curvature

The classical theories for beams and plates assume small deformations. That is, the definition of the radius of curvature, ρ , shown in Fig. 2.6 can be linearised as the second derivative of the deflection, w'' ; see Eq. 2.1. This assumption yields a 1% inaccuracy if the slope, w' , does not exceed 0.08 rad, corresponding to less than 5 degrees [6]. Additional considerations on

the validity of the assumption can be found in [PIII].

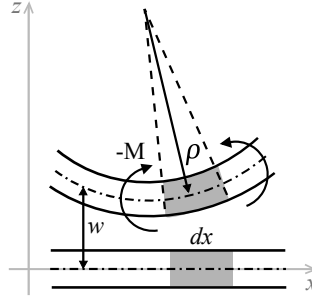


Figure 2.6. Radius of curvature in the bending of a straight bar. Modified from Bazant et al. [6].

$$\frac{1}{\rho} = \frac{w''}{(1+w'^2)^{\frac{3}{2}}} \approx w'' \quad (2.1)$$

This linearisation affects the governing differential equations of motion, as it appears in the definition of the strain, as $\epsilon = z/\rho$. Therefore, the definition of the bending moment becomes:

$$M(x) = \int_A z \sigma dA = -E \int_A \epsilon z dA = -E \int_A \frac{z^2}{\rho} dA = -\frac{EI}{\rho} = -EIw''. \quad (2.2)$$

where $I = \int_A z^2 dA$ is the principal moment of inertia of a cross-section of area A .

2.3.2 Von Kármán kinematics

The von Kármán kinematics is briefly introduced for the case of a plate in the $(x-y)$ plane. Further information can be found in the literature; see, e.g., [71]. Beginning from the Green-Lagrange strain tensor, the tensor components are defined as:

$$E_{jk} = \frac{1}{2} \left(\frac{\delta u_j}{\delta x_k} + \frac{\delta u_k}{\delta x_j} + \frac{\delta u_m}{\delta x_j} \frac{\delta u_m}{\delta x_k} \right), \quad j, k = 1, 2, 3. \quad (2.3)$$

The classical plate theory states that straight lines normal to the middle plane remain straight and normal to the middle plane during deformation. This implies that the vertical and shear strains ϵ_z , γ_{xz} and γ_{yz} can be neglected. Moreover, higher-order terms of the form $\delta^2(u_1, u_2, u_3)/\delta(x, y)^2$ are neglected. Assuming an initial distortion w_0 , by replacing $u_{1,2,3}$ with:

$$u_1 = u - z \frac{du_3}{dx} \quad (2.4)$$

$$u_2 = v - z \frac{dv_3}{dy} \quad (2.5)$$

$$u_3 = w + w_0, \quad (2.6)$$

the von Kármán strains are derived as:

$$\varepsilon_{xx} = \frac{dw}{dx} + \frac{1}{2} \left(\frac{dw}{dx} + \frac{dw_0}{dx} \right)^2 - z \frac{d^2w}{dx^2} = \varepsilon_{xx}^0(x, y) + z \cdot \varepsilon_{xx}^1(x, y), \quad (2.7)$$

$$\varepsilon_{yy} = \frac{1}{2} \left(\frac{dw}{dy} + \frac{dw_0}{dy} \right)^2 - z \frac{d^2w}{dy^2} = \varepsilon_{yy}^0(x, y) + z \cdot \varepsilon_{yy}^1(x, y), \quad (2.8)$$

$$\gamma_{xy} = \left(\frac{dw}{dx} + \frac{dw_0}{dx} \right) \left(\frac{dw}{dy} + \frac{dw_0}{dy} \right) - z \frac{d^2w}{dxdy} = \gamma_{xy}^0(x, y) + z \cdot \gamma_{xy}^1(x, y), \quad (2.9)$$

with $\gamma_{xy} = 2\varepsilon_{xy}$. In the above equations, w_0 is assumed small compared to the thickness and does not generate additional curvature, i.e., w_0 does not appear in ε^1 terms.

2.3.3 2D plate theory

This study assumes a linear-elastic material. Therefore, Hooke's law is used to define the stress-strain constitutive equations:

$$\sigma_{xx} = \frac{E}{1-\nu^2} (\varepsilon_{xx} + \nu\varepsilon_{yy}), \quad (2.10)$$

$$\sigma_{yy} = \frac{E}{1-\nu^2} (\varepsilon_{yy} + \nu\varepsilon_{xx}) \quad (2.11)$$

$$\tau_{xy} = G\gamma_{xy}, \quad (2.12)$$

where the stress in the thickness direction, σ_z , is considered negligible, i.e. plane stress condition is assumed given the small thickness of the plate.

Considering the given constitutive relations and strain definitions, the generalised governing differential equations are derived according to the principle of virtual displacement based on the minimisation of the total potential energy; see, e.g., [71]. The potential energy, $\Pi(x, y)$, is defined as:

$$\Pi(x, y) = \iiint_V \Psi(x, y) dx dy dz - W_{ext}, \quad (2.13)$$

where $W_{ext}(x, y)$ is the external work, which, in this case, is only done by the uni-axial load, P , i.e., $W_{ext} = (P\delta u)$, and $\Psi(x, y)$ is the energy density function indicated in Eq. 2.14.

$$\Psi(x, y) = \frac{1}{2} \sigma_{ij}(x, y) \varepsilon_{ij}(x, y) \quad (2.14)$$

The bending governing differential equation is derived by replacing stresses and strains, and by considering the definitions of the membrane forces, N_{ij} , and bending moments, M_{ij} , as stress resultants integrated through the thickness, i.e.:

$$N_{ij} = \int_{-t/2}^{t/2} \sigma_{ij} dz \quad \text{and} \quad M_{ij} = \int_{-t/2}^{t/2} z \cdot \sigma_{ij} dz. \quad (2.15)$$

Moreover, for an isotropic material:

$$\begin{Bmatrix} M_{xx} \\ M_{yy} \\ M_{xy} \end{Bmatrix} = D_p \begin{bmatrix} 1 & \nu & 0 \\ \nu & 1 & 0 \\ 0 & 0 & \frac{1-\nu}{2} \end{bmatrix} \begin{Bmatrix} \varepsilon_{xx}^1 \\ \varepsilon_{yy}^1 \\ \gamma_{xy}^1 \end{Bmatrix}, \quad (2.16)$$

where $D_p = Et^3/12(1-\nu^2)$. With an initial deformation, w_0 , the total deflection is the sum of w_0 and the deflection, w_1 , due to external loading, i.e., $w = w_1 + w_0$. Using the relation in Eq. 2.16 and $N_{xx} = P$, the governing equation is obtained as:

$$\frac{\partial^4 w_1}{\partial x^4} + 2 \frac{\partial^4 w_1}{\partial x^2 \partial y^2} + \frac{\partial^4 w_1}{\partial y^4} = \frac{1}{D_p} P \frac{\partial^2 (w_1 + w_0)}{\partial x^2}, \quad (2.17)$$

where the presence of the initial deformation can be seen as a fictitious load equivalent to $P(\partial^2 w_0 / \partial x^2)$ [42]. The plate is modelled as simply-supported (SS) over its edges of length l and width b ; see Fig. 2.7.

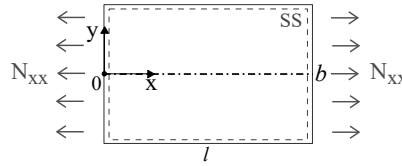


Figure 2.7. Simply-supported plate under uni-axial tension $N_{xx} = P$ over the x -direction.

This allows for a closed-form solution, which is well-known and given by Timoshenko [72]. This solution uses a double trigonometric series, satisfying the boundary conditions and the initial distortion shape. Accordingly:

$$w_0 = \sum_{m=1}^{\infty} \sum_{n=1}^{\infty} a_{mn} \sin \frac{m\pi x}{l} \cos \frac{n\pi y}{b} \quad (2.18)$$

and

$$w_1 = \sum_{m=1}^{\infty} \sum_{n=1}^{\infty} b_{mn} \sin \frac{m\pi x}{l} \cos \frac{n\pi y}{b}, \quad (2.19)$$

with $(a, b)_{mn}$ series coefficients associated to wavelength (a/m) and (b/n) . By substitution of Eqs. 2.18 and 2.19 in Eq. 2.17:

$$b_{mn} = \frac{-a_{mn} N_{xx}}{D_p \left(\frac{\pi}{l^2}\right)^2 \left(m + \frac{n^2}{m} \left(\frac{l^2}{b^2}\right)\right)^2 + N_{xx}}. \quad (2.20)$$

Considerations on the modelling assumptions are given in [PII]. The described model is applied to panels that are geometrically symmetric about the centre line, as the one shown in Fig. 2.1.

2.3.4 1D beam theory

The development of a 1D beam analytical solution stems from the need for highly simplified models similar to those currently provided by the IIW recommendations [5]. To reach such a level of simplification, additional assumptions on the joint geometry are needed. Firstly, the analytical model neglects the distortion in the transverse direction, i.e. the beam represents a distorted profile in the longitudinal direction of the plates. Moreover, the distortion is assumed symmetric with respect to the weld, as in Fig. 1.6. The symmetry allows for considering only one side of the joint by including an ideal clamp in the weld location, as shown in Figure 2.8. Considering only the distortion in the vicinity of the weld, the shape is described by superimposing a linear lateral sway, $w_{y_0}(x)$ of amplitude y_0 , and a half-sine curvature, $w_{a_0}(x)$, with maximum mid-length amplitude a_0 , which is:

$$w_0(x) = w_{y_0}(x) + w_{a_0}(x) = \frac{y_0 x}{l} + a_0 \sin\left(\frac{\pi x}{l}\right). \quad (2.21)$$

The local angle, α_l , is defined as in Eq. 2.22; see Fig. 2.8. Considering the angle definition in the IIW recommendations in Fig. 1.6 [5], the angle α_g in Fig. 2.8 corresponds to half of the global angular misalignment, i.e., $\alpha_g = \alpha_G/2$. Similarly, $\alpha_l = \alpha_L/2$ ².

$$\alpha_l = \alpha_{a_0} + \alpha_{y_0} = \arctan\left(\frac{a_0 \pi}{l}\right) + \arctan\left(\frac{y_0}{l}\right) \quad (2.22)$$

The end opposite to the weld location undertakes the axial load P end has *fixed or pinned* BC.

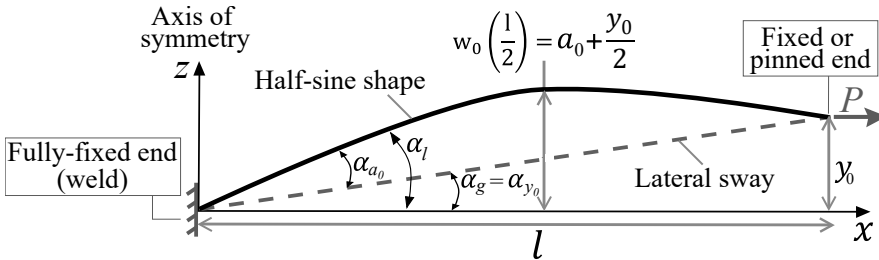


Figure 2.8. Idealised beam model of a welded distorted thin plate under tension ($P > 0$).

To include the effect of the geometrical non-linearity, the model considers the von Kármán kinematics. As for the plate model, the principle of virtual displacement is used, and a closed-form solution is available thanks to the slope-deflection method for statically indeterminate beams [73]. The solution is shown in [PIII].

Once the beam is solved, the stress magnification factor is computed as $k_m = \sigma_{hs}/\sigma_n$. The structural hot-spot stress is the sum of the membrane

²Notice that in [PIII] angles α_l and α_g are called α_L and α_G , respectively.

stress, σ_m , and bending stress, σ_b , defined as:

$$\begin{cases} \sigma_m(x) = \frac{P}{bt} \\ \sigma_b(x) = \frac{M(x)z}{I} = \frac{M_a t}{I} \end{cases}, \quad (2.23)$$

where the hot-spot, indicated as point a , is located at $z = t/2$ and $x = 0$. The obtained k_m -factor formulations are indicated in Table 2.1 and 2.2.

Table 2.1. Stress magnification factor (k_m) formulations from [PIII]. $C1$ and $C2$ coefficients are defined in Table 2.2.

	Pinned BC	Fixed BC
k_{m,loc,a_0}	$1 + \frac{6\gamma_0}{t} \frac{\tanh(\beta)}{\beta} + \frac{6\alpha_0\pi\beta\tanh(\beta)}{t(\pi^2+\beta^2)}$	$1 + \frac{3\gamma_0}{t} \frac{\tanh\left(\frac{\beta}{2}\right)}{\frac{\beta}{2}} + \frac{6\alpha_0\pi\beta}{t(\pi^2+\beta^2)\tanh\left(\frac{\beta}{2}\right)}$
k_{m,loc,α_L}	$1 + 3\alpha_G \frac{1}{t} (C1_p - C2_p) + 3\alpha_L \frac{1}{t} C2_p$	$1 + 3\alpha_G \frac{1}{t} (C1_f - C2_f) + 3\alpha_L \frac{1}{t} C2_f$

Table 2.2. $C1$ and $C2$ coefficients for the computation of the k_m factor using global (α_G) and local (α_L) angles.

Pinned BC	Fixed BC
$C1_p = \frac{\tanh(\beta)}{\beta}$	$C1_f = \frac{\tanh\left(\frac{\beta}{2}\right)}{\beta}$
$C2_p = \frac{\beta\tanh(\beta)}{(\pi^2+\beta^2)}$	$C2_f = \frac{\beta}{(\pi^2+\beta^2)\tanh\left(\frac{\beta}{2}\right)}$

2.4 Semi-analytical modelling of the weld rigidity

The model described in the previous section reduces the hot spot to a point located at the origin of the beam. This neglects the weld profile which can introduce significant inaccuracy in the presence of a large weld bead. The latter can deform, thus violating the assumption of an ideally rigid clamp. Moreover, the end opposite to the weld may also experience a non-ideal, or intermediate, boundary condition. Therefore, elastic bending connections with relative stiffness parameters k_a and k_b are included at the two ends of the beam. Based on [PIV], the variation in the rotational stiffness at the end opposite to the weld does not have a significant influence on the stress concentration at the weld location. Hence, k_b is not considered, and an ideal boundary condition can be assigned to this end.

In representing the weld rigidity, the rotational stiffness k_a can vary between zero and infinity and is computed as:

$$k_a = -\frac{M_a}{\theta_a}, \quad (2.24)$$

where θ_a is the spring rotation.

In order to avoid singularities in the calculations, fixity factors ranging between 0, for a pinned connection, and 1, for a rigid connection, are used to describe the rotational constraint. The fixity factor is defined as:

$$\rho_a = \frac{\Phi_a}{\Phi_a + \theta_a}, \quad (2.25)$$

where Φ_a is the rotation of the beam with flexural stiffness EI/l ; see Fig. 2.9.

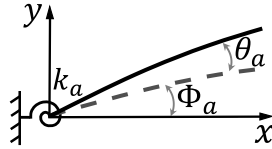


Figure 2.9. Definition of the beam rotation angle (Φ_a) and the spring rotation angle (θ_a) at the left end (a) of the beam.

For an ideal simply supported beam under external end moments M_a and M_b , M_a is solved as [74]:

$$M_a = \frac{EI}{l} \Phi_a \left[4 \left(1 + 0.5 \frac{\Phi_b}{\Phi_a} \right) \right]. \quad (2.26)$$

In Eq. 2.26, the term in square brackets can be replaced by b^* , which contributes to the correction of the beam flexural stiffness when the angle ratio Φ_b/Φ_a becomes $(\Phi_b + \theta_b)/(\Phi_a + \theta_a)$. In this study, $\theta_b = 0$, thus the ratio is $\Phi_b/(\Phi_a + \theta_a)$. Assuming ideal boundary conditions, $b^*_{(1)(2)} = 4$, and $b^*_{(3)(4)} = 3$, for constrained and free rotation, respectively. Using these values in the fixity factor definition:

$$\rho_a = \frac{\Phi_a}{\Phi_a + \theta_a} = \frac{1}{1 + \frac{\theta_a}{\Phi_a}} = \frac{1}{1 + \frac{-M_a b^* EI}{k_a M_a l}} = \frac{1}{1 - \frac{b^* EI}{k_a l}}, \quad (2.27)$$

and

$$k_a = \frac{b^* EI}{\frac{1}{\rho_a} - 1} l, \quad (2.28)$$

which enters the beam formulation via the slope boundary conditions.

2.4.1 Computation of the fixity factors

The computation of the fixity factor is based on a 2D FE 4-nodes S4 shell element-based model. The thickness of the shell elements is uniform and equal to the plate width, b_p . The elements are aligned to the x-y plane to study possible stress non-linearity through the thickness. With an element aspect ratio of 1 [75], their length in the x-direction is 0.35 mm and is reduced to 0.2 mm near the weld. The mesh is shown in Fig. 2.10 in a view cut including the weld region, where the red lines indicate the model

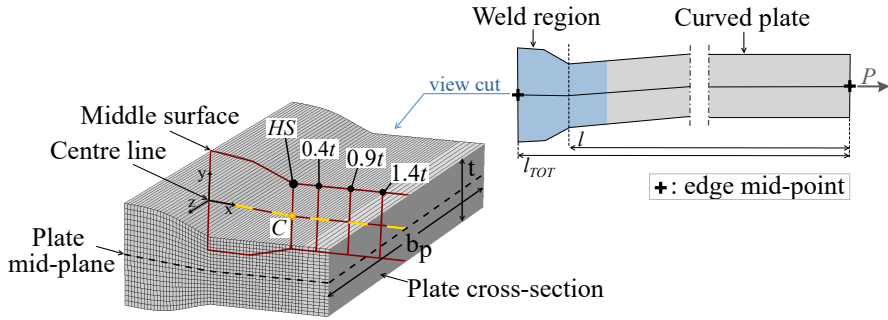
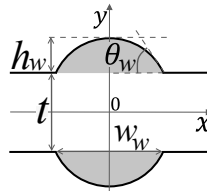


Figure 2.10. 2D symmetric FE model of welded plates and a view cut near the weld region. The geometry and mesh distribution are shown, along with definitions and locations of interest for the present analysis.

profile at the middle surface of the shell elements. One side of a symmetric butt-joint is modelled, as shown in Fig. 2.10. The geometry parameters are shown in Table 2.3 for a small (SB), medium (MB), and large (LB) weld bead. The area of the weld toe and root is typically approximated as $w_w h_w / 2$. In the table, the term $area_N$ provides such a number normalised by the base plate area ($w_w t$).

Table 2.3. Weld beads dimensions based on the idealised weld profile.

	Weld bead	w_w [mm]	h_w [mm]	θ_w [deg]	$area_N$
	SB	2.6	0.3	13	0.075
	MB	5	0.5	20	0.125
	LB	10.6	1.5	30	0.375

The weld width is varied for the SB and LB models, while the variation of θ_w and h_w is studied on the MB model. Two different global-to-local angle ratios of the distortion are selected, i.e., $\alpha_l/\alpha_g = [2, 5]$, with $\alpha_g = 2.5$ deg.

The plate curvature considered in the model is based on the simplified shape in Eq. 2.10. The curvature starts at the cross-section between the weld region and the plate and the boundary conditions over the side edges are applied at the mid-points shown in Fig. 2.10 by using a coupling interaction between these points and the edges. A clamp over the left edge simulates the weld symmetry, while the opposite edge is subjected to tension, P , equivalent to [100, 200, 300] MPa. The transverse displacement in the z -direction is constrained for the whole model, which is in plane stress condition, i.e., $\sigma_z = 0$, and assumes linear-elastic material properties.

Among commonly accepted approaches for the numerical estimation of the structural hot-spot stress [5], the through-thickness linearisation (TTL) and the quadratic extrapolation (QE) approaches are chosen, as they were shown to be more appropriate in earlier studies [31]. In TTL, the non-linear

distribution of the stress near the weld is linearised based on the linear stress distribution away from the weld [76]. The QE approach, instead, extrapolates the hot-spot stress by using the stresses, σ , at points located at $(0.4, 0.9, 1.4) \cdot t$ from the weld line in Eq. 2.29; see Fig.2.10. Further details on these approaches can be found in [PV].

$$\sigma_{hs} = 2.52\sigma_{0.4t} - 2.24\sigma_{0.9t} + 0.72\sigma_{1.4t} \quad (2.29)$$

3. Results and Discussion

The main outcome of this study is the successful reduction in scale when modelling distorted panels using the numerical and analytical approaches discussed in Chapter 2. The accuracy of these approaches was evaluated by comparing them to the 3D GNL-FEA analyses of the distorted panels described in Section 2.2.2 and validated in [PI]. The following sections present and discuss the panel geometries, the results obtained for 2D and 1D numerical models in [PII], the analytical formulations in [PIII], and the semi-analytical approach from [PIV] and [PV].

Given that the experimental validation of the 3D GNL-FEA could only be conducted for the panels after cutting, the numerical study is conducted on the distortions obtained after the panels were cut from the demo block. Some considerations about the distortions obtained through in-situ measurements on the block are given in the general notes in Section 4.

3.1 Geometry characterisation

Five panels were cut from the ship-deck demo block shown in Fig. 1.2. The block was built in the EU RAMSSES project by Meyer Turku Oy [77] and measures $12 \times 7 \times 2.7$ m. Each cut panel has longitudinal HP80 \times 5 stiffeners and T440 \times 7/150 \times 10 T-beams as transverse frames. The panel's plates are 4 mm-thick, 3360 mm-long and 586 mm-wide, with a total cross-sectional area of 3424 mm². The laser-MAG hybrid weld is located at 2097 mm from the left of the panel. Considering the plate field geometry shown in Fig. 2.1, $l_{p,1} = 1740$ mm, $l_{p,2} = 818.5$ mm, and $b_p = 456$ mm. Detailed component dimensions are given in [PII], where panels are identified in two types: P1 and P2. P1-type panels, i.e., P1.1, P1.2, and P1.3, have a transverse butt joint in the plate field, while P2-type panels, i.e., P2.1 and P2.2, present an additional longitudinal weld; see black dashed lines in Fig. 3.1(a). The figure shows two examples of the contour of the measured distortions over the panel plate field, while Fig. 3.1(b) shows the centre line distortions from the scans before and after cutting or before

and after clamping for testing [PI].

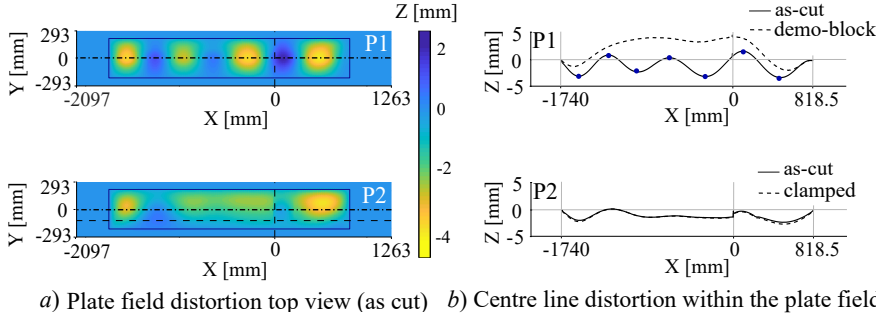


Figure 3.1. Examples of (a) Contour plots for panel types P1 and P2, and (b) comparison of the panel centre line in ‘as-cut’ and ‘demo-block’ or ‘as-cut clamped’ configuration. Modified from [PII].

The weld beads were measured to be from 3.5 to 5 mm-wide. Considering the peak of the weld toe as the zero on the X-axis, Table 3.1 indicates the coordinates of the right and left weld lines, $X_{w,r}$ and $X_{w,l}$, respectively. In the table, the maximum initial distortion in absolute value, $|w_{0,max}|$, and the maximum span of the initial distortion, $\Delta w_0 = \max(w_0) - \min(w_0)$, are included for all the panels. For all of them, the span is measured between consecutive peaks and valleys of the distortion.

Table 3.1. Right, $X_{w,r}$, and left, $X_{w,l}$, weld line coordinates, absolute maximum initial distortion, $|w_{0,max}|$, and maximum span of the distortion profiles, Δw_0 .

Specimen	P1.1	P1.2	P1.3	P2.1	P2.2
$X_{w,l}$ [mm]	-2.5	-1.7	-2.5	-1.5	-1.5
$X_{w,r}$ [mm]	2.5	1.8	2.5	3.5	2.5
$ w_{0,max} $ [mm]	2.20	3.77	3.63	2.60	3.70
Δw_0 [mm]	3.71	5.05	5.40	2.71	2.19

Referring to the classifications on the severity of the distortions introduced in Section 1.1.3 and by applying the tolerance limits defined by Hughes et al. [36], the panel geometry leads to:

$$w_{0,max} \text{ [mm]} = \begin{cases} 0.47 & \text{slight level} \\ 1.88 & \text{average level,} \\ 5.64 & \text{severe level} \end{cases} \quad (3.1)$$

where $w_{0,max}$ refers to the amplitude of a distortion. In the measured distortions, the amplitude can be considered both in terms of maximum distance from the X-axis and as the span between peaks and valleys. Considering both the absolute maximum distortions and distortion spans in

Table 3.1, the geometries considered in the study are from average to severe quality based on Eq. 3.1, and within the tolerance limit given by the IACS [78]. Given that these distortions gradually straighten under tensile load, the small-deflection theories and the principle of linear superposition of the initial distortion to the developing deflection can be applied. Nevertheless, the superposition principle is generally valid when the distortion is smaller than the thickness, meaning that for the principle to be fully applicable, the largest distortions should first be straightened to some extent. This is further discussed in Section 3.2.

In general, even for distortions within normally acceptable tolerances [36, 78], curved distortion shapes modify the overall stress distribution, which makes the current assessment recommendations unsuitable for the thin-walled components. From Fig. 3.1(b), it can be observed that the distortion profiles do not fall under any of the typical distortion profiles presented in Fig. 1.3. Therefore, the validity of the mentioned commonly accepted distortion tolerances might need revision in the case of multi-buckled shapes with variable amplitudes, as in the present study.

3.2 From 3D FEA to 2D analytical solution

To simplify the GNL-FEA of the distorted panels, the 3D shell element-based model described in Section 2.2.2 is used as a reference to evaluate the accuracy of the 2D FE models of the distorted plate fields without the stiffening frame. Figure 3.2 presents the ratio of structural stress to nominal stress obtained from the panel model compared to plate models with, w , and without, nw , the weld geometry for nominal stresses of 25 and 250 MPa. The w -plate is as described in Section 2.2.3, while the nw -plate solution comes from the plate theory in Section 2.3.3, where a 19-term trigonometric series describes the distortion in the longitudinal direction while a simple half-wave is modelled in the transverse direction [PII].

The w -plate model is very accurate regardless of the load applied, meaning that the modelling of the stiffening frame is not necessary in the structural stress analysis of the distorted plate field. On the contrary, the nw -plate, which also neglects the weld cross-section, is less accurate under low load and ignores the local stress concentration around the weld location. Therefore, weld modelling is necessary for the evaluation of local stresses, while the plate analytical solution can only be used to predict the global stress distribution in terms of stress peaks and valleys away from geometric discontinuities.

The accuracy of the nw -plate solution in the global stress estimation is shown in Fig. 3.3, which refers to the locations of the stress peaks and valleys indicated by full dots (for the bottom surface) and empty dots (for the top surface) in Fig. 3.2.

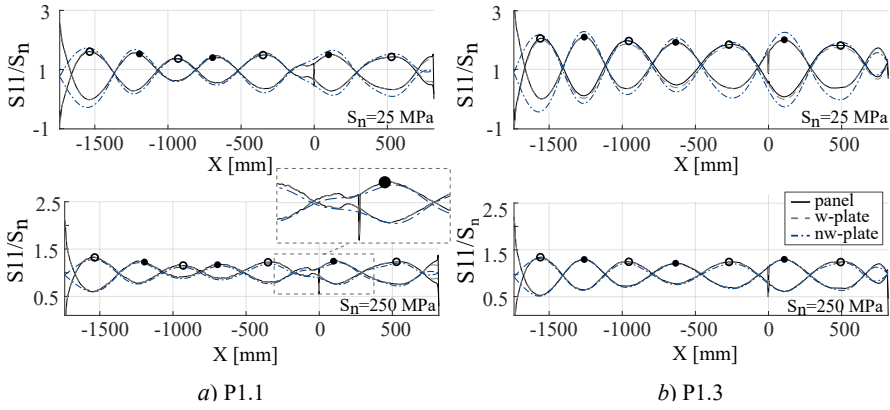


Figure 3.2. Comparison of the structural (S_{11}) to nominal (S_n) stress ratio in models *Panel*, *w-plate*, and *nw-plate* under 25 and 250 MPa. Empty and filled dots indicate peak stress centre line locations of top and bottom surfaces, respectively.

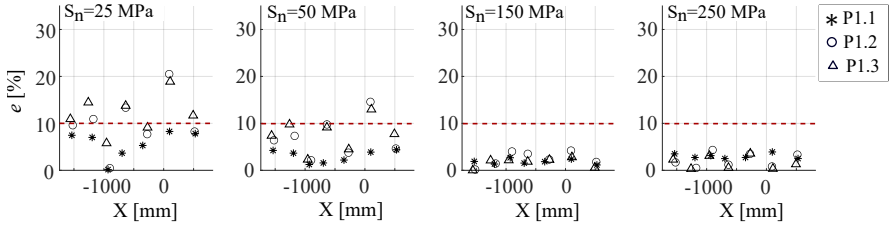


Figure 3.3. Absolute error percentage for P1-type panels for loads of 25, 50, 150, and 250 MPa at the peak stress locations indicated in Fig. 3.2.

Figure 3.3 indicates an absolute error of less than 10%-error for the analytical solution under a load of at least 50 MPa and less than 5% for $S_n \geq 150$ MPa. As mentioned in the previous section, for the analytical plate solution to be applied, the initial distortion should be smaller than the plate thickness. For instance, this is not the case for distortions in P1.2 and P1.3. Therefore, the inaccuracy of the analytical solution is larger at lower loads and decreases as the load increases and the panels gradually straighten. In case of relatively large distortions, there can be significant effects on the plate field dimensions, and higher-order non-linear curvature terms associated with w_0 should be included in the strain-displacement relationship in Section 2.3.2; see Steen et al. [38]. Nevertheless, this factor does not constitute a major source of error when significant straightening of the distortion occurs due to applied tension. On the contrary, a relevant source of error is the approximation over the Y-direction, which uses a simple half-wave, $\cos(\pi y/b)$, meaning that n is always equal to 1 in Eq. 2.18. A second-order cosine function, $\cos^2(\pi y/b)$, shown to be a better approximation in Fig. 3.4, would not be suitable for a closed-form solution. The figure includes a parabolic approximation for comparison.

The study presented in [PII] showed that the error percentage for the *nw-plate* model tends to have exponential growth with the maximum absolute

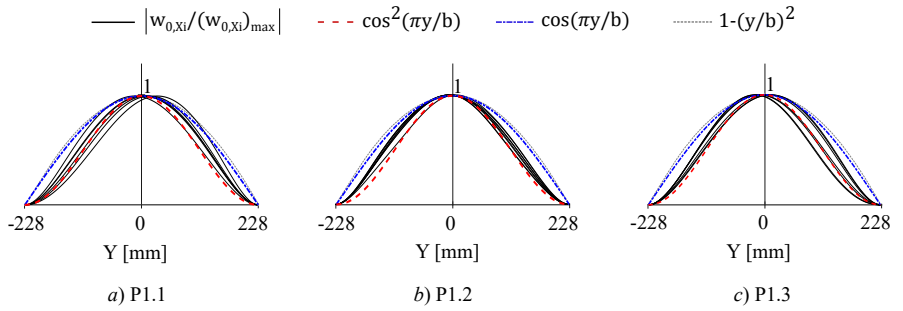


Figure 3.4. Comparison between measured distortions and analytical approximations along the Y direction. The absolute values of the measured data (black lines) are normalised with their maximum at relative peak amplitude locations (X_i) along the X direction; peak amplitude locations are indicated with blue dots in Fig. 3.1b).

value of the initial slope of the plate field distortion, $|\delta w_0/\delta x|_{max}$, for panels P1.1, P1.2, and P1.3 under 150 MPa; see Fig. 3.5(b). The error grows similarly with the maximum span of the initial distortion, $\Delta w_{0,max}$, as shown in Fig. 3.5(a). Nevertheless, the slope values seem to follow the same trend regardless of the distortion shapes, thus being a more representative parameter than the maximum amplitude in the characterisation of the distortions. The shapes considered lead to inaccuracy of the analytical plate model lower than 10% for a maximum slope of 0.02 rad (i.e., ~ 1.5 deg) under 150 MPa and is in correspondence of maximum amplitudes approaching the plate thickness.

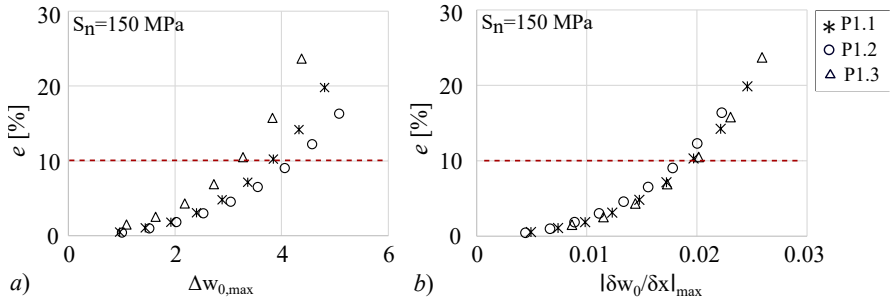


Figure 3.5. Error percentage plotted as a function of the absolute value of the maximum slope of the analytical solution compared to the numerical solution of a simply-supported, distorted plate under 150 MPa.

The straightening effect due to the tensile load is shown in Fig. 3.6 as the ratio between the maximum span of the deformed configuration over the plate thickness, i.e., $\Delta(w_1 + w_0)_{max}/t$. The straightening occurs similarly in all the panels, being more pronounced in those with larger initial distortion amplitudes that generate larger secondary bending moments on the plates. Based on Figs. 3.3 and 3.6, for the given distortions, the plate solution results in less than 10% error when $\Delta(w_1 + w_0)_{max} < t$.

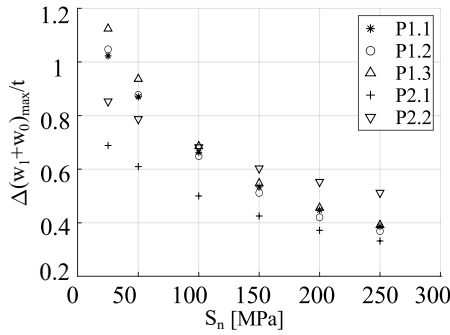


Figure 3.6. Maximum span to thickness ratio of the distorted configuration, $(w_1 + w_0)_{max}/t$, as a function of the nominal applied load for all panel specimens over their centre line.

3.3 From 3D to 1D finite element analysis

Given that the plate model including the well cross-section, i.e., *w-plate*, is shown to provide very consistent results with the panel model in Fig. 3.2, the next step in the simplification of the GNL-FEA of the distorted plate field is to reduce the modelling scale to one dimension. Therefore, a 1D FE model is first used to represent the entire centre line of the distorted panel, including the weld cross-section. Figure 3.7 indicates the maximum error in the proximity of the weld and at the first stress peak location from the weld defined at ± 10 mm, e_{10} , and ± 500 mm, e_{500} , respectively.

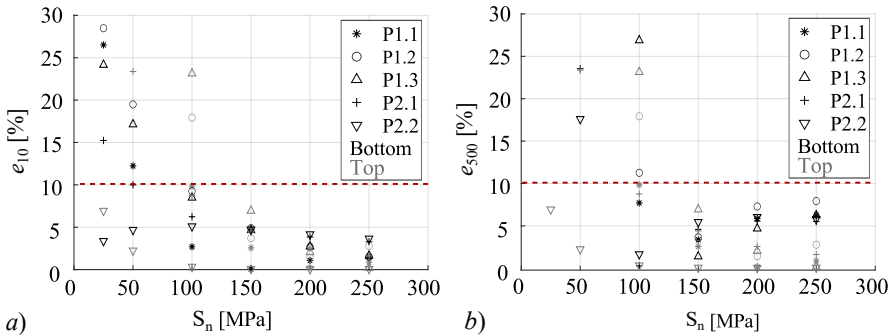


Figure 3.7. Error percentage in the numerical stress estimation of the 1D beam model against the panel model *a)* within 10 mm (e_{10}) and *b)* 500 mm (e_{500}) from the weld location. Missing data beyond $e_{10,500} = 35\%$ are not shown.

Less than 10% error is found when the panel is subject to a stress ≥ 150 MPa, that is an imposed axial displacement of at least 1.5 mm on the beam. Referring to Fig. 3.6, such a condition means straightening of the distortions below $0.6 \times t$, relating to a maximum slope of 0.015 rad (i.e., ~ 0.86 deg).

Beam translation over the plate width - The asymmetry about the centre line for panels P2.1 and P2.2 that can be seen in Fig. 3.1 is

due to the longitudinal weld. Nevertheless, even in the panels where geometric symmetry about the centre line is fulfilled, i.e., P1.1, P1.2, and P1.3, a slight asymmetry of the distortion appears due to, e.g., uneven misalignment over the weld line. Therefore, the use of the 1D GNL-FEA for distortion profiles at a distance from the centre line is investigated. The study considers profiles at $Y_t = [50, 100, 150, 175]$ mm; see a model example in Fig. 2.5(a). Only positive values of Y_t are used to select the profiles that would be more critical in terms of structural stress concentrations.

Figure 3.8 shows the error in stress within ± 500 mm from the weld location for P1.1 and P2.1 under 100, 150, and 250 MPa. The results

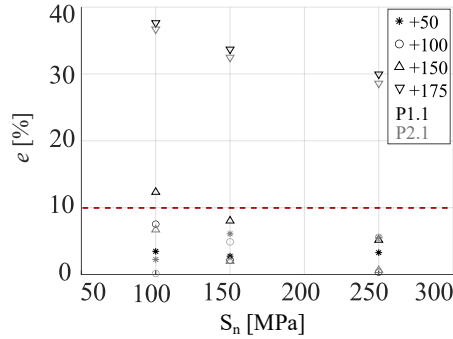


Figure 3.8. Error percentage due to the beam translation over the plate width at $Y_t = [50...175]$ mm for panels P1.1 and P2.1 under 100, 150, and 250 MPa.

indicate that the beam model can simulate the panel stress over longitudinal profiles up to ± 150 mm, i.e., $\pm 30\%$ -distance, from the centre line. By contrast, the error increases considerably for the beam model representing the distortion profile at ± 175 mm, i.e., closer to the plate edges.

Spatial truncation of the distortion - Considering that the recently proposed analytical formulations for curved butt-welded thin plates generally assume a simple initial curvature, the next results assess the accuracy of the 1D GNL-FEA when the distortion profile is truncated at $X_t = [100, 200, 400]$ mm, i.e., the distortion is reduced up to maximum a single buckle on both sides of the weld; see Fig. 2.5(b).

Figure 3.9 shows the error within 50 mm from the weld. The shortest observation window for an acceptable accuracy of the beam model is within ± 200 mm from the weld in the longitudinal direction. Nevertheless, the first buckle on each side of the weld should be included because it is responsible for the highest stress peak. Considering that the first buckling mode has a wavelength that is typically similar to the plate aspect ratio, b_p/L , [71], it is advisable to model the distortion within a

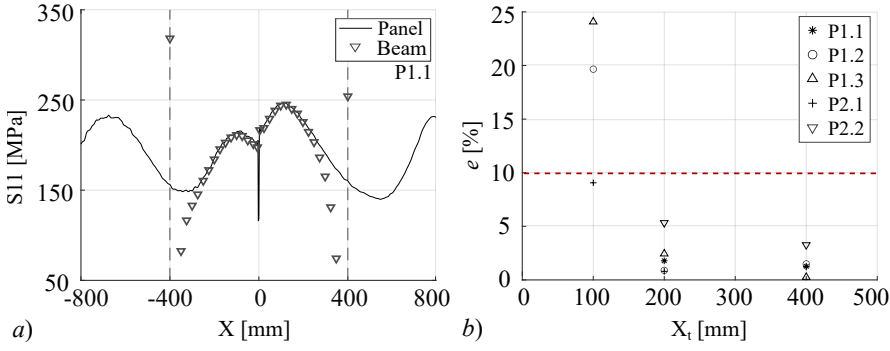


Figure 3.9. a) Stress comparison between panel model and beam with spatial truncation of the distortion at $X_t=400$ mm for panels P1.1; and b) maximum error percentage within 50 mm away from the weld of the beam with truncation at $X_t = [100, 200, 400]$ mm for all panels.

span approaching the width of the plate. This represents about ± 400 mm in the present panels. The results open the possibility of adapting an analytical formulation like the one presented in Section 2.3.4.

3.4 1D analytical model

Spatial truncation of the distortion reveals that the structural stress concentration near the weld is mainly due to the shape of the distortion up to its first buckle. Therefore, the validity range of the analytical formulations developed in this work (see Section 2.3.4) and the related improvement compared to the current IIW recommendations can be studied considering a simple curvature near the weld.

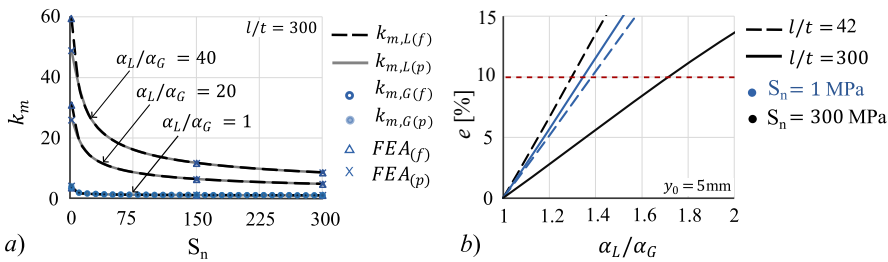


Figure 3.10. a) numerical (FEA) and analytical $k_{m,L}$ factor comparison, including the IIW formulation, $k_{m,G}$, for different angle ratios and both pinned, p , and fixed, f , BCs; b) percentage difference between the $k_{m,L}$ and $k_{m,G}$ as a function of the local-to-global angle ratio when $y_0 = 5$ mm and under fixed BCs.

The proposed solutions, assuming a half-sine curvature and von Kármán kinematics, are verified against the GNL-FEA of an equivalent FE beam model. The case for a slender ratio of $l/t = 300$ is shown in Fig. 3.10(a). In the figure, $k_{m,G}$ indicates the global angular stress magnification factor

for fixed BCs based on the IIW recommendations in Table 1.1; while $k_{m,L}$ refers to the local angular stress magnification factor for fixed BCs proposed in this work and given in Table 2.1. These factors are compared for different local-to-global angle ratios, α_L/α_G , defined so to be equal to 1 in the case of a flat shape as in Fig. 1.6. Figure 3.10(b) shows the percentage difference between the $k_{m,L}$ and $k_{m,G}$ under fixed BCs for different slenderness ratios at varying angle ratio. Based on the results in the figure, the error percentage related to the IIW formulation increases as the local-to-global angle ratio increases. Depending on the beam slenderness ratio, a 10% error is reached between around $\alpha_L/\alpha_G = 1.25$ and 1.75. By contrast, the $k_{m,L}$ factor presented in this work can predict the structural stress concentration for a broader range of angle ratios given that the distortion is well-approximated by the superposition of a linear lateral sway and a half-sine curvature.

3.5 The influence of the weld profile

The analytical formulations for a simply-curved beam with non-ideal BCs, implemented in [PIV] and used in the semi-analytical study in [PV], showed a maximum of 3% error in structural hot-spot stress prediction compared to a 2D FE model of the welded plate introduced in Section 2.4.1.

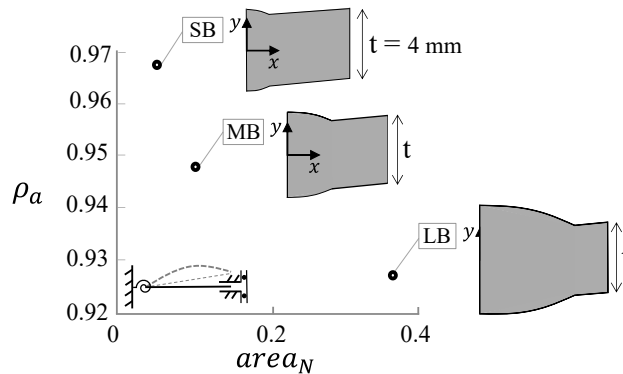


Figure 3.11. Comparison between fixity factors (ρ_a) for different weld normalised areas ($area_N$) considering fixed rotational constraint at the end opposite to the weld location; see Table 2.3.

Figure 3.11 shows the computed fixity factors, ρ_a , considering small (SB) medium (MB), and large (LB) weld bead profiles described by the weld normalised areas, $area_N$; see Table 2.3.

In [PV], the fixity factors computed semi-analytically range between 0.92 and 1. The variability of these factors mainly depends on the weld width, the effect of which is shown in Fig. 3.12, where the ideal case of $\rho_a = 1$ is indicated by a red triangle.

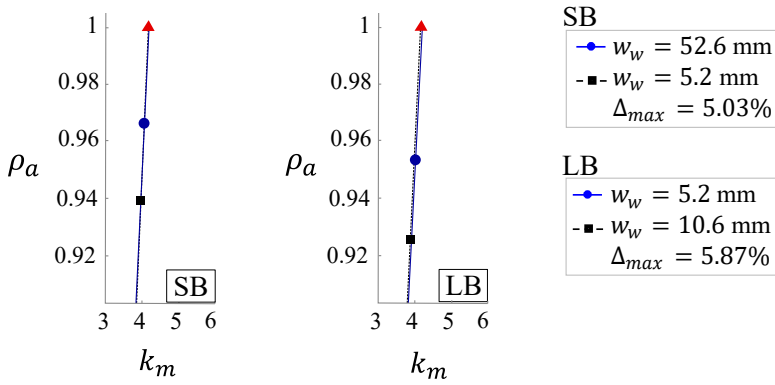


Figure 3.12. Stress magnification factor, k_m , as a function of the fixity factor, ρ_a , for different widths of the weld bead for SB and LB models with fixed rotational constraint at the end opposite to the weld. Δ_{max} is the maximum percentage difference between the k_m factor for $\rho_a = 1$ and the computed ρ_a .

Using the computed fixity factors the stress magnification factors differed by less than 6% compared to assuming $\rho_a = 1$. The overlap between the solid and dashed lines, indicating shorter and wider welds, respectively, suggests that the weld geometry does not affect the k_m factor to the same extent as load levels and angle ratios; see [PV].

Overall, the variation in the stress magnification factor caused by a variation of the fixity factor between 0.92 and 1 is small, especially in the case of very slender components. Nevertheless, assuming $\rho_a = 1$ may cause up to 9% overestimation of the stress compared to using a non-ideally rigid constraint, suggesting that, in the case of very large welds, the computation of a fixity factor might need to be considered. The same conclusion has been claimed by Shen et al. [79].

4. General remarks and future work

Chapter 3 presented a systematic decrease in the modelling scale of distortions in stiffened panels, while ensuring structural stress predictions within a 10% error margin from the reference model determined using a 3D FE panel model with plate field distortion. Although the highly simplified analytical beam models have been derived from the point of view of small-scale butt-joint specimens, as typically done in the fatigue assessment of welded connections [5], the present thesis contributes to bridging the gap between scales. The model with spatial truncation of the distortion presented in Section 2.2.4 is a step forward in such a direction. This model is shown to reach good accuracy in terms of local structural stress assessment of the butt-welded area of the panels. In the case of multi-buckled distortion shapes, it resulted in good accuracy when the ratio between the maximum span of the deformed configuration over the plate thickness, i.e., $\Delta(w_1 + w_0)_{max}/t$, is less than 0.6. Concerning the analysis of the global stress distribution, the analytical plate model is preferable for capturing the stress distribution in the transverse direction, and it is shown to be reliable for $(w_0 + w_1)/t < 1$. These ranges were found for an initial maximum slope of the distortion around 0.02 rad (i.e., ~ 1.5 deg) and would change depending on the irregularity of the distortion, i.e., its waviness. This confirms the need to consider both amplitude and shape in the characterisation of the distortions on thin plates in panels, as indicated in earlier numerical studies [68].

In general, despite being conservative under low loads, the simplified models were found accurate when loads above 100 MPa were applied to the panel structure. Although this is strictly related to the characteristics of the distortion and its straightening, the mentioned load range is relevant in the context of the fatigue assessment of these panels. This is shown in Fig. 4.1, which represents an estimation of the critical load range under long-term variable loading following a two-parameter Weibull distribution and the Palmgren-Miner's fatigue damage definition [36], as given by DNV [7]. The calculation considers the fatigue resistance against structural hot-spot stress of the welded joint described by bi-linear S-N curves with

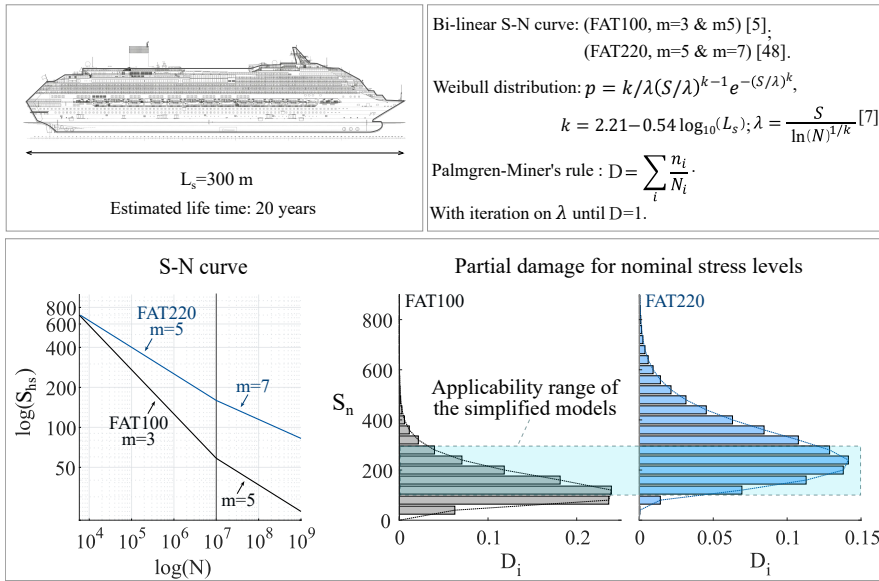


Figure 4.1. Simplified fatigue analysis for the estimation of the significant load range under long-term variable loading.

knee point at $N = 10^7$ cycles. Two curves are shown: from the current IIW recommendation [5], i.e., FAT100 with slope $m=3$ and $m=5$, and from the full-scale experimental observation on high-quality thin-walled panels by Lillemäe et al. [50], i.e., FAT220 with slope $m=5$ and $m=7$. This simplified fatigue analysis is presented for a generic large ship with a total length, L_s , of 300 m and a lifetime of 20 years. From Fig. 4.1, it can be observed that the applicability range of the presented modelling approaches covers the load levels critical to the fatigue performance of the structure in the elastic range of the material and within the small-deformation regime, especially considering the experimental S-N curve for thin-walled panels. A summary of the use of the different modelling strategies is given in Fig. 4.2 and Table 4.1.

Several works have been published since 2018 using 1D analytical models and simply curved shapes. Similar to the formulation presented by the current author in [PIII], other formulations have also produced improvements to the modelling of curved distortions. Although all are based on the Euler-Bernoulli beam theory with the assumption of von-Kármán kinematics, some differences in the shape approximation and derivation are reflected in the k_m factor computation. In particular, Zhou et al. [57] have modelled global and local angular distortions through equivalent notional (or dummy) loads acting at the mid-span of an ideally straight beam and depending on the curvature slopes at the beam ends, while Shen et al. [59] have modelled the initial curvature with a polynomial quadratic function. The first model is more versatile in terms of shape configuration

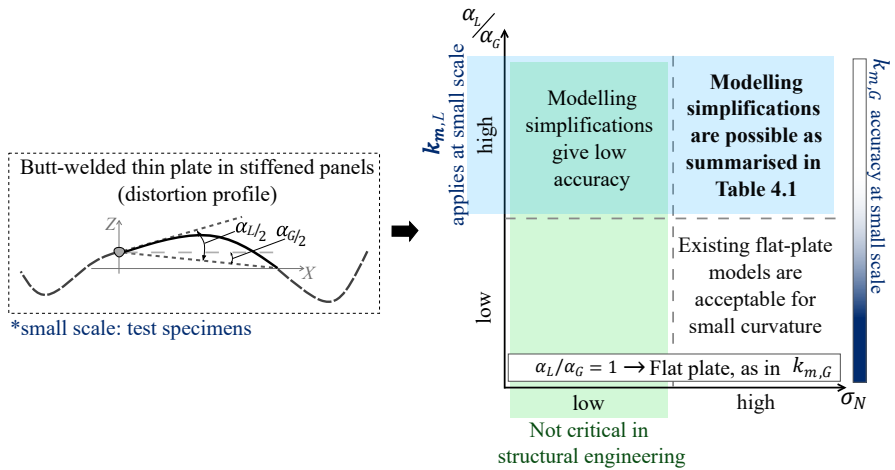
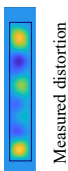
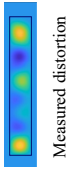
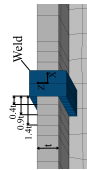
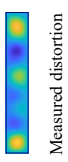
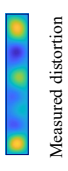
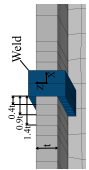
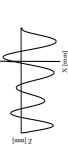
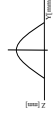
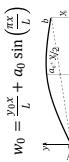
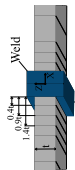
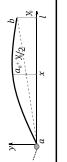
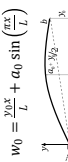
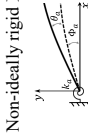


Figure 4.2. The use of modelling strategies for thin-walled stiffened panels with an initial distortion. Notes on the modelling of small-scale butt-welded specimens are also indicated, referring to analytical k_m formulations for local, L, and global, G, angular misalignment.

but implies a few additional terms in the formulation, thus being more challenging in its engineering use compared to the other solutions. The second model is relatively more concise, but the definition of the quadratic function is less immediate in engineering practices, where the measure of local angles is a challenge. Moreover, the order, and so the number of coefficients for the distortion function, would grow quickly when needing to describe more complex distortions. Compared to these formulations, the one proposed in [PIII] presents an effective engineering tool for its conciseness, and the assumption of a sinusoidal shape function is in line with the theoretical description of typical distortion shapes [2], which makes the formulation easy to extend to more complex distortions. Overall, predictions for slender components showed negligible differences among these formulations [PIII]. Nonetheless, the different beam models are verified numerically, and experimental validation is still needed to assess their suitability for engineering applications.

Table 4.1. Summary of the simplified modelling strategies proposed in the present work and their applicability for local and global structural stress assessment of the distorted plate field in stiffened panels..




MODELLING APPROACH	FORMULATION	DISTORTION IN X-DIRECTION	DISTORTION IN Y-DIRECTION	WELD	STIFFENING FRAME	LOCAL	GLOBAL	ADDITIONAL NOTES
3D GNL-FEA (shell-element based assembly)	S4R NLGEM	 Measured distortion	 Measured distortion		Ideally-straight shell-element parts	✓	✓	NoE: 137870 CPU Time: 33.0 s The modelling requires more dimensional informations.
2D GNL-FEA	S4R NLGEM	 Measured distortion	 Measured distortion		Rigid rotational constraint	✓	✓	NoE: 47564 CPU Time: 11.0 s Equivalent to panel model in assessing the plate field distortion.
2D CPT	Von Kármán strain definition	Trigonometric series approximation of measured distortion 	$w_0(x,y) = w_0(x) \cdot \cos\left(\frac{\pi y}{b}\right)$ 	Neglected	Neglected (simply-supported edges)	✗	✓	Trigonometric approximation can be adapted to a wide set of distortions.
1D GNL-FEA	B31 NLGEM	Measured distortion 	Neglected		Neglected	✓	✗	NoE: 517 CPU Time: 0.4 s Distortion truncation and spatial translation are possible.
1D EBT	Second-order Euler-Bernoulli Beam	Measured distortion $w_0 = \frac{\gamma_0 x^2}{L} + a_0 \sin\left(\frac{\pi x}{L}\right)$ 	Neglected	Ideal clamp	Neglected	✗	✗	Accurate for small-scale specimens. Requires future work for adaptation to panels.
1D EBT (with weld rigidity effect)	Second-order Euler-Bernoulli Beam with non-ideal constraint	Measured distortion $w_0 = \frac{\gamma_0 x^2}{L} + a_0 \sin\left(\frac{\pi x}{L}\right)$ 	Neglected		Neglected	✗	✗	Accurate for small-scale specimens. An estimation of the fixity factor is needed.

S4R: four-noded shell elements with reduced integration (Abaqus)

B31: beam element (Abaqus)

NLGEM: geometric nonlinear analysis (Abaqus)

NoE: Number of Elements

 applicable
 not applicable
 requiring future research

Prior to this current study, the k_m formulations mentioned above have not been extended to the structural hot-spot stress assessment of panel structures. To suggest a way of performing such an extension and draw a direction for future developments on the topic, the author has adapted the analytical formulation derived in [PIII] and the one available in the IIW recommendations to the panel distortions considered in [PII]. Before the analysis is shown, the mentioned analytical formulations are reported in Table 4.2. From the table, it is possible to observe that the developed formulation, $k_{m,L}$, consists of a linear superposition of the existing IIW formulation, $k_{m,G}$, for linear lateral sway of amplitude y_0 and a term dependent on the amplitude of the half-sine curvature, a_0 .

Table 4.2. Stress magnification factor formulations from IIW recommendations [5] and [PIII], considering fixed BC.

Fixed BC	
IIW [5]	$k_{m,G} = 1 + \frac{3y_0}{t} \frac{\tanh\left(\frac{\beta}{2}\right)}{\frac{\beta}{2}}$
PIII	$k_{m,L} = 1 + \frac{3y_0}{t} \frac{\tanh\left(\frac{\beta}{2}\right)}{\frac{\beta}{2}} + \frac{6a_0\pi\beta}{t(\pi^2 + \beta^2)\tanh\left(\frac{\beta}{2}\right)}$

In the adaptation of the analytical model to the panel distortions, the maximum amplitude of the distortion within its first buckle from the weld location can be considered in defining the term a_0 in Table 4.2. This is shown in Fig. 4.3 for the plate on the right side of the panel transverse weld.

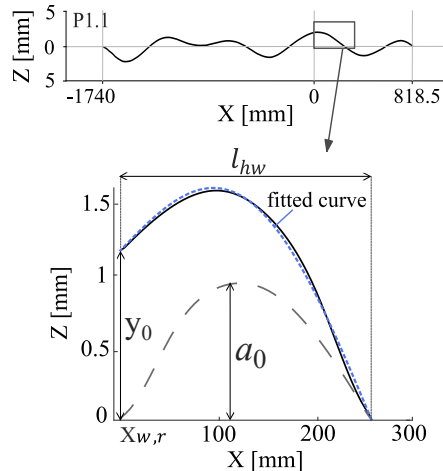


Figure 4.3. Misalignment definition in the adaptation of the analytical model in [PIII] to the panel distortions in Fig. 3.1

In this analysis, centre line profiles for the demo-block (db) panels P1.2 and P1.3 are available and considered along with the profiles for panels P1.1,

P1.2, and P1.3. The set of measured misalignments for the computation of the stress magnification factors is summarised in Table 4.3.

Table 4.3. Misalignments measured for panels within the first half-wave on the right side of the welded joint; see Fig. 4.3

Panel	l_{hw} [mm]	e [mm]	y_0 [mm]	a_0 [mm]
P1.1	255.6	0.08	1.10	0.95
P1.2	215.6	0.03	0.54	1.27
P1.3	250.6	0.14	0.69	1.38
P1.2db	305.6	0.30	3.15	0.21
P1.3db	370.6	0.10	3.5	1.19

In applying the formulations, a fixed boundary condition at the loaded end of the beam is assumed. Moreover, given that the panels do not present a low-quality weld profile and have very slender plates, the beam end corresponding to the weld location does not need to account for a non-ideal rotational constraint, i.e., for a fixity factor $\rho \neq 1$.

Linear extrapolation of the numerical solution from the panel is compared to the beam analytical solution by considering a beam slenderness coefficient under applied tension equal to $\beta = (2L/t)\sqrt{3(\sigma_n(1 - \nu^2)/E)}$, where L is the total panel length; see Fig. 2.1. Moreover, while the axial and angular misalignments are computed based on the length of the considered plate, the contribution of local angular misalignment is computed on the length, l_{hw} , of the half-wave in Fig. 4.3. The numerical results computed between 25 and 250 MPa indicated stress magnification factors ranging between 1.05 and 1.5. These results are used to evaluate the accuracy of the analytical formulations.

Figure 4.4(a) compares the stress magnification factors based on the presented analytical beam model, $k_{m,L}$, and the ones based on the IIW recommendations, $k_{m,G}$, by presenting their error percentage with respect to the k_m factors extrapolated from the panel GNL-FEA. In Fig. 4.4(b), the two analytical formulations are verified against the GNL-FEA of a 1D model of the centre line distortion up to l_{hw} ; see [PIII] for the model details under fixed boundary conditions.

Figure 4.4(a) suggests that the IIW formulation underestimates the stress concentration, although being in an acceptable range of -10% error. By comparison, the proposed formulation gives accurate but slightly conservative results in most cases. For the case of small-scale models, Fig. 4.4(b) clearly shows that the curvature has a non-negligible effect on the stress magnification factor, thus making the IIW formulations ineffective. In light of this, it is concluded that the IIW formulation for flat distortions is in an acceptable range for the panel because of an error compensation related to the stiffness of the panel model and the flat distortion compared to

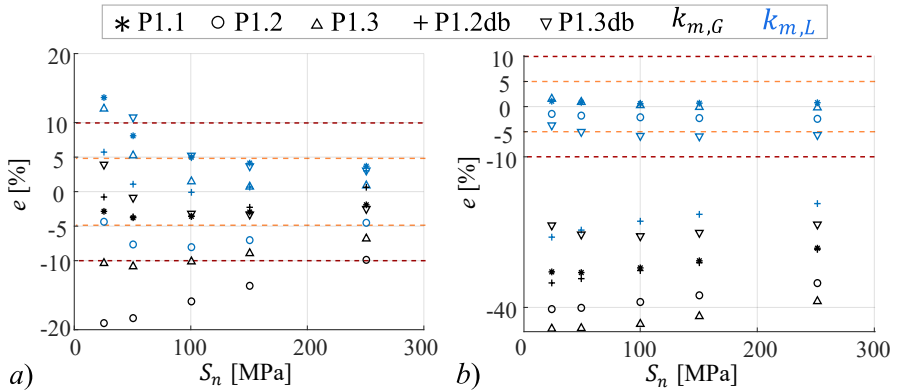


Figure 4.4. Percent difference between the numerical k_m factors from (a) stiffened panel models and (b) 1D numerical model of the panel distortion up to l_{hw} compared to the analytical $k_{m,L}$ and $k_{m,G}$ factors Table 4.2.

the curved distortion. However, the compensation is nonphysical, and thus cannot be generally assumed, and it is not enough for a safe estimation of the stress concentration in the cases considered.

4.1 Ideas for future research directions

Referring to Fig. 4.4, the error in the structural stress prediction may vary according to the method and accuracy in defining the distortion. Therefore, a deeper investigation into the adaptation of simply-curved beam models to the panels is needed in the future. Moreover, modelling the weld rigidity via, e.g., a rotational spring as in [PV], may be required to release the assumption of symmetry about the weld toe in the analytical beam model.

Based on this study, and to develop the presented modelling strategies further, future research should focus on:

- the implementation of an automated process from distortion measurement to stress magnification factor evaluation;
- the experimental validation of simplified analytical beam models and the elaboration of a standard protocol to measure the local angular misalignment at the weld location;
- and a generalisation to any panel dimension and distortion shape aimed at understanding the limitations of the assumptions behind the presented modelling strategies.

Regarding the experimental validation of the simplified analytical models, a contribution in this direction has been given by Sandgren [80], who

conducted an experimental validation of the formulation presented in this work for thin and slender butt-welded small-scale specimens. The specimens were tested under tension after scanning the initial distortion. The error percentage between the analytical formulation developed in this work and the experimental structural hot-spot stress remained mostly below 10%. However, exceptions were observed, suggesting that further investigations are needed.

About the generalisation of the presented modelling approaches, similar to the work of Georgiadis and Samuelides [81] and as an extension of the work by Tatsumi and Kageyama [82], a statistical analysis of the distortion patterns could be used to validate the spatial truncation approach and the following assumption on the half-sine curvature shape of the simplified analytical formulations.

As mentioned in Section 1.2.2, this study does not explicitly consider mean stresses, considering prevalent hogging conditions in passenger ships. However, structural changes in lightweight superstructures may lead to different weight distribution and, thus, bending mechanisms. Therefore, future work is needed to broaden the validity of the approaches by considering the effect of both compressive and tensile mean stresses, and related non-linear secondary bending actions, on the structure. A transition from compressive to tensile mean stress could contribute to changes in the distortion shape that are difficult to predict. This may lead to a computationally complex analysis, especially in the case of small amplitude distortions when bending-dominated areas over the distorted plate field are not easily identified.

Eventually, similar simplified modelling strategies can be developed to include residual stresses and material non-linearity. The latter could be an opportunity to address uni-axial compression loading and approach the buckling instability of welded plates in ship structures. In such a case, the role of the weld in terms of non-ideal rotational constraint as in [PV] could play a more significant role in modelling local changes in the joint stiffness [83, 84, 85]. Moreover, the contribution of the stiffening frame requires additional considerations due to possible local buckling phenomena [37, 39, 44, 86]. This explains why the presented results have not been extended in a straightforward manner to the case of compression.

In general, considering the advances in welding technologies in the shipbuilding industry [87], the severity of local distortions is expected to decrease significantly, thus enhancing the structural integrity of ships and supporting the use of highly-simplified, yet representative, models in limit states analyses of these structures.

5. Conclusions

From an economic and engineering perspective, the simplest action towards lightweight ship superstructures is the use of thin plates, so that the traditional modular design and production lines can be maintained, while simultaneously achieving significant weight reduction.

In designing thin-walled ship decks, there is the need to consider the irregularity rising in the welding-induced distortions on the stiffened panel units, which consequently show different mechanical responses compared to panels made of relatively thick plates.

Due to the lack of early-design assessment tools accounting for complex distortions, in ship design, the effect of distortion-induced stress concentrations on the fatigue strength of thin decks is generally evaluated by the GNL-FEA of 3D complex models. Based on the established use of stress magnification factors, k_m , formulations for flat welding-induced distortions as proposed by the IIW, the development of improved k_m factors or highly-simplified assessment tools for non-flat distortions is an attractive solution.

In this regard, this thesis presented a characterisation of welding-induced distortions of thin plates on 4-mm full-scale ship-deck stiffened panels and proposed simplified modelling strategies for a more efficient structural stress assessment under uni-axial tension. The suitability of simplifications was addressed in a gradual scale reduction from a 3D shell element-based GNL-FEA to a 1D analytical model.

Based on the present study, due to the shape irregularity, the characterisation of the distortions for the local structural assessment requires the consideration of the local curvature in terms of slope and should not be limited to their maximum amplitude, as typically done in considering the ultimate strength of these structures. As a consequence, available analysis methods and distortion tolerances do not necessarily apply in case of irregular distortions.

Nevertheless, the geometric complexity does not hinder the possibility of developing simplified assessment methods. The analysis of the distortion effects on the panel under tension does not require the modelling of

the stiffening frame. Moreover, when the global stress distribution is of interest, even the weld geometry can be fully neglected. By contrast, for a local assessment in the vicinity of the weld, the model geometry can be simplified to a rectangular cross-section thicker than the welded plates, and 1D beam element-based models can be used to simulate the stress concentration over a distorted profile within 60% of the width of the plate field. Furthermore, modelling the distortion up to its first buckle from the weld location in the longitudinal direction guarantees a reliable representation of the stresses near the weld. This finding suggests that there is a possibility to adapt the analytic formulations developed in the current work, derived from a simply-curved Euler-Bernoulli beam model, to the panel analysis. Compared to the current IIW recommendations, depending on the severity of the misalignment, curved beam models can improve the accuracy in stress prediction by more than 10% in the presence of curved distortions. In this work, the beam model was implemented in a semi-analytical approach to account for the weld rigidity in terms of a non-ideal rotational constraint. This approach is considered valuable in the case of relatively large weld widths and non-slender plates.

Although this thesis focused on ship deck stiffened panels, the modelling principle and geometry considerations presented can also be applied to a broader range of structural problems dealing with macro-geometric imperfections. This includes the waviness of bars in lattices [88, 89, 90] or the waviness of fibres in composites [91, 92]. However, the quantitative results are verified for the case studies selected throughout the study and are limited to the macro-geometric distortions of the panel plate field, without considering the effects of residual stresses, material non-linearity, and additional distortions in the stiffening frame of the panel.

References

- [1] J. Harvey Evans. Basic design concepts. *Journal of the American Society for Naval Engineers*, 71(4):671–678, 1959.
- [2] J.K. Paik and A.K. Thayamballi. *Ultimate Limit State Design of Steel-Plated Structures*. Wiley, 2003.
- [3] K. kyun, B. Imjun, P. Bee Yee, and S. Sung-Chul. A useful guide of effective mesh-size decision in predicting the ultimate strength of flat-and curved plates in compression. *Journal of Ocean Engineering and Science*, 8(4), 2023.
- [4] D. Radaj, C. M. Sonsino, and W. Fricke. *Fatigue assessment of welded joints by local approaches*. Woodhead publishing, 2006.
- [5] E. Niemi, W. Fricke, and S.J. Maddox. Structural hot-spot stress approach to fatigue analysis of welded components. iiw doc. 13, 2018.
- [6] Z.P. Bazant, L. Cedolin, and J.W. Hutchinson. *Stability of Structures: Elastic, Inelastic, Fracture, and Damage Theories*, volume 60. 1993.
- [7] Det Norske Veritas (DNV). Fatigue assessment of ship structures., 2021. <https://standards.dnv.com/explorer/document/E809ABA5B1984646A243729A0A0AD44D>.
- [8] Det Norske Veritas (DNV). <https://www.dnv.com/rules-standards/index.html> (accessed Feb. 14, 2024).
- [9] International Maritime Organization (IMO). <https://www.imo.org/en/About/Pages/DocumentsResources.aspx> (accessed Feb. 14, 2024).
- [10] International Organization for Standardization (ISO). <https://www.iso.org/standards.html> (accessed Feb. 14, 2024).
- [11] Bureau Veritas (BV). <https://marine-offshore.bureauveritas.com/rules-guidelines> (accessed Feb. 14, 2024).
- [12] I. Lillemäe, H. Remes, and J. Romanoff. Influence of initial distortion of 3 mm thin superstructure decks on hull girder response for fatigue assessment. *Marine Structures*, 37:203–218, 2014.
- [13] J. Romanoff, H. Remes, P. Varsta, B. Reinaldo Goncalves, M. Kõrgesaar, I. Lillemäe-Avi, Jelovica J., and S. Liinalampi. Limit state analyses in design of thin-walled marine structures - some aspects on length-scales. *Offshore Mechanics and Arctic Engineering*, 142:1–21, 2019.
- [14] F. Czerwinski. Current trends in automotive lightweighting strategies and materials. *Materials*, 14(21), 2021.

- [15] L. Zhu, N. Li, and P.R.N. Childs. Light-weighting in aerospace component and system design. *Propulsion and Power Research*, 7(2):103–119, 2018.
- [16] P. Noury, B. Hayman, D. McGeorge, and J. Weitzenböck. Lightweight construction for advanced shipbuilding-recent development. *Proceedings of the 37th WEGEMT summer school*, pages 11–15, 2002.
- [17] J.R. Weitzenböck, B. Hayman, D. Hersvik, G. and McGeorge, P. Noury, D.M. Hill, and A. Echtermeyer. Application of composites in ships and offshore-a review and outlook. In *Royal Institution of Naval Architects-International Conference on Marine and Offshore Composites*, pages 1–39, 2010.
- [18] M. Kutsuna, S. Kitamura, K. Shibata, H. Sakamoto, and K. Tsushima. Improvement of the joint performance in laser welding of aluminium alloys. *Welding in the World*, 50:22–27, 2006.
- [19] J. Beaudet, G. Rückert, and F. Cortial. Fatigue behavior of fsw high-yield strength steel welds for shipbuilding application. *Welding in the World*, 63(5):1369–1378, 2019.
- [20] J.M. Gordo and C. Guedes Soares. Tests on ultimate strength of hull box girders made of high tensile steel. *Marine Structures*, 22(4):770–790, 2009.
- [21] H. Lillemäe, I. and Remes, S. Liinalampi, and A. Itävuo. Influence of weld quality on the fatigue strength of thin normal and high strength steel butt joints. *Welding in the World*, 60:731–740, 2016.
- [22] J. Romanoff, H. Naar, and P. Varsta. Interaction between web-core sandwich deck and hull girder of passenger ship. In *11th International Symposium on Practical Design of Ships and Other Floating Structures, Rio de Janeiro, RJ, Brazil, 20-24.09.2010*, pages 1071–1078, Brazil, 2010. COPPE. VK: T20404.
- [23] D. Frank, J. Romanoff, and H. Remes. Fatigue strength assessment of laser stake-welded web-core steel sandwich panels. *Fatigue & Fracture of Engineering Materials & Structures*, 36(8):724–737, 2013.
- [24] K. Liu, S. Zong, Y. Li, Z. Wang, Z. Hu, and Z. Wang. Structural response of the u-type corrugated core sandwich panel used in ship structures under the lateral quasi-static compression load. *Marine Structures*, 84:103198, 2022.
- [25] G. Palomba, G. Epasto, L. Sutherland, and V. Crupi. Aluminium honeycomb sandwich as a design alternative for lightweight marine structures. *Ships and Offshore Structures*, 17(10):2355–2366, 2022.
- [26] P. Gallo, M. Guglielmo, J. Romanoff, and H. Remes. Influence of crack tip plasticity on fatigue behaviour of laser stake-welded t-joints made of thin plates. *International Journal of Mechanical Sciences*, 136:112–123, 2018.
- [27] M. Li, R. Yan, W. Shen, K. Qin, J. Li, and K. Liu. Fatigue characteristics of sandwich composite joints in ships. *Ocean Engineering*, 254:111254, 2022.
- [28] J. Sun and K. Dilger. Influence of welding sequence and external restraint on buckling distortion in thin-plate arc-welded joints. *Journal of Advanced Joining Processes*, 8:100157, 2023.
- [29] M. Ghafouri, A. Ahola, J. Ahn, and T. Björk. Numerical and experimental investigations on the welding residual stresses and distortions of the short fillet welds in high strength steel plates. *Engineering Structures*, 260:114269, 2022.
- [30] M. Hashemzadeh, Y. Garbatov, and C. Guedes Soares. Hybrid-laser welding-induced distortions and residual stresses analysis of large-scale stiffener panel. *Ocean Engineering*, 245:110411, 2022.

- [31] H. Remes, J. Romanoff, I. Lillemäe, D. Frank, S. Liinalampi, P. Lehto, and P. Varsta. Factors affecting the fatigue strength of thin-plates in large structures. *International Journal of Fatigue*, 101:397–407, 2017.
- [32] M.S. Yi, D.H. Lee, H.H. Löee, and J.K. Paik. Direct measurements and numerical predictions of welding-induced initial deformations in a full-scale steel stiffened plate structure. *Thin-Walled Structures*, 153:106786, 2020.
- [33] L. Eggert, W. Fricke, and H. Paetzold. Fatigue strength of thin-plated block joints with typical shipbuilding imperfections. *Welding in the World*, 56:119–128, 2012.
- [34] Y. Ueda and T. Yao. The influence of complex initial deflection modes on the behaviour and ultimate strength of rectangular plates in compression. *Journal of Constructional Steel Research*, 5:265–302, 1985.
- [35] J.K. Paik, A.K. Thayamballi, and D.H. Kim. An analytical method for the ultimate compressive strength and effective plating of stiffened panels. *Journal of Constructional Steel Research*, 49(1):43–68, 1999.
- [36] O.F. Hughes, D. Béghin, and J.K. Paik. *Ship Structural Analysis and Design*. Knovel Library. Society of Naval Architects and Marine Engineers, 2010.
- [37] J.K. Paik, A.K. Thayamballi, and B.J. Kim. Large deflection orthotropic plate approach to develop ultimate strength formulations for stiffened panels under combined biaxial compression/tension and lateral pressure. *Thin-Walled Structures*, 39(3):215–246, 2001.
- [38] E. Steen, E. Byklum, and J. Helleland. Elastic postbuckling stiffness of biaxially compressed rectangular plates. *Engineering Structures*, 30:2631–2643, 2008.
- [39] J.K. Paik and J.K. Seo. Nonlinear finite element method models for ultimate strength analysis of steel stiffened-plate structures under combined biaxial compression and lateral pressure actions—part i: Plate elements. *Thin-Walled Structures*, 47(8-9):1008–1017, 2009.
- [40] L. Gannon, Y. Liu, N. Pegg, and M.J. Smith. Effect of welding-induced residual stress and distortion on ship hull girder ultimate strength. *Marine Structures*, 28:25–49, 2012.
- [41] Z. Shengming. A review and study on ultimate strength of steel plates and stiffened panels in axial compression. *Ships and Offshore Structures*, 11(1):81–91, 2016.
- [42] S.P. Timoshenko and J.M. Gere. *Theory of Elastic Stability*. Dover Publications, 2012.
- [43] E. Byklum and J. Amdahl. A simplified method for elastic large deflection analysis of plates and stiffened panels due to local buckling. *Thin-Walled Structures*, 40:925–953, 2002.
- [44] L. Brubak, J. Helleland, and E. Steen. Semi-analytical buckling strength analysis of plates with arbitrary stiffener arrangements. *Journal of Constructional Steel Research*, 63:532–543, 2007.
- [45] L. Brubak and J. Helleland. Strength criteria in semi-analytical, large deflection analysis of stiffened plates in local and global bending. *Thin-Walled Structures*, 46:1382–1390, 2008.
- [46] J.K. Paik, B.J. Kim, and J.K. Seo. Methods for ultimate limit state assessment of ships and ship-shaped offshore structures: Part iii hull girders. *Ocean Engineering*, 35:281–286, 2008.

- [47] J.K. Paik. Large-deflection and ultimate strength behavior of stiffened panels and grillages. *Thin-Walled Structures*, pages 301–331, 03 2018.
- [48] P.P. Chaithanya, P.K. Das, A. Crow, and S. Hunt. The effect of distortion on the buckling strength of stiffened panels. *Ships and Offshore Structures*, 5(2):141–153, 2010. doi: 10.1080/17445300903331818.
- [49] IACS. Shipbuilding and repair quality standard, 2017. N.47,p.21.
- [50] I. Lillemäe, S. Liinalampi, H. Remes, A. Itävu, and A. Niemelä. Fatigue strength of thin laser-hybrid welded full-scale deck structure. *International Journal of Fatigue*, 95:282–292, 2017.
- [51] I. Lotsberg. *Fatigue Design of Marine Structures*. Cambridge University Press, 2016.
- [52] W. Fricke. Recent developments and future challenges in fatigue strength assessment of welded joints. *Proceedings of the Institution of Mechanical Engineers, Part C: Journal of Mechanical Engineering Science*, 229:1224–1239, 2014. doi: 10.1177/0954406214550015.
- [53] D. Radaj, C.M. Sonsino, and W. Fricke. Recent developments in local concepts of fatigue assessment of welded joints. *International Journal of Fatigue*, 31(1):2–11, 2009.
- [54] Y. Kuriyama, Y. Saiga, T. Kamiyama, and T. Ohno. Low-cycle fatigue strength of butt welded joints with angular distortion. *International Institute of Welding (IIW)*, 1971.
- [55] S.J. Maddox and International Institute of Welding. *Fitness-for-purpose Assessment of Misalignment in Transverse Butt Welds Subject to Fatigue Loading*. Doc / International Institute of Welding. Welding Institute, 1985.
- [56] I. Lillemäe-Avi, H. Remes, Y. Dong, Y. Garbatov, Y. Quemener, and E. Eggert. Benchmark study on considering welding-induced distortion in structural stress analysis of thin-plate structures. *Progress in the Analysis and Design of Marine Structures*. London: Taylor & Francis Group, pages 387–394, 2017.
- [57] W. Zhou, P. Dong, I. Lillemäe, and H. Remes. A 2nd-order scf solution for modeling distortion effects on fatigue of lightweight structures. *Weld World*, 2019.
- [58] P. Dong, W. Zhou, and S. Xing. An analytical method for interpreting distortion effects on fatigue test results of thin plate panel specimens. *Weld World*, 63:1707–1714, 2019.
- [59] W. Shen, Y. Qiu, C. Li, Y. Hu, and M. Li. Fatigue strength evaluation of thin plate butt joints considering initial deformation. *International Journal of Fatigue*, 125:85–96, 2019.
- [60] W. Fricke and O. Feltz. Consideration of influence factors between small-scale specimens and large components on the fatigue strength of thin-plated block joints in shipbuilding. *Fatigue & Fracture of Engineering Materials & Structures*, 36:1223–1231, 2013.
- [61] Germanischer Lloyd. Comparison of no.47 shipbuilding and repair quality standard with japan shipbuilding quality standard and production standard of the german shipbuilding industry. GL-SAJ-IACS-VSM-Shipbuilding Standards.doc.
- [62] A. Kendrick. The effect of fabrication tolerances on fatigue life of welded joints. Technical report, Ship Structure Committee, SSC-436, 2004.

- [63] S. Chen, S. Xie, T. Li, and J. Wang. Acceptance levels of misalignment of welded joints under different quality categories. *Journal of Constructional Steel Research*, 212:108247, 2024.
- [64] H. Naar. *Ultimate strength of hull girder for passenger ships. Doctoral dissertation*. Helsinki University of Technology, 2006.
- [65] I. Lillemäe, H. Lammi, L. Molter, and H. Remes. Fatigue strength of welded butt joints in thin and slender specimens. *International Journal of Fatigue*, 44:98–106, 2012.
- [66] H. Remes and W. Fricke. Influencing factors on fatigue strength of welded thin plates based on structural stress assessment. *Welding in the World*, 58:915–923, 2014.
- [67] W. Fricke, H. Remes, O. Feltz, I. Lillemäe, D. Tchuindjang, T. Reinert, A. Nevierov, W. Sichermann, M. Brinkmann, T. Kontkanen, B. Bohlmann, and L. Molter. Fatigue strength of laser-welded thin-plate ship structures based on nominal and structural hot-spot stress approach. *Ships and Off-shore Structures*, 10:39–44, 2015. doi: 10.1080/17445302.2013.850208.
- [68] H. Lillemäe, I. Lillemäe, and J. Romanoff. Influence of initial distortion on the structural stress in 3mm thick stiffened panels. *Thin-Walled Structures*, 72:121–127, 2013.
- [69] ATOS. Atos compact scan. <https://www.gom.com/en/products/3d-scanning/atos-compact-scan> (accessed Feb. 14, 2024).
- [70] ABAQUS online documentation: Version 6.6-1. 2006. <https://shorturl.at/ghoK0> (accessed Feb. 14, 2024).
- [71] J.N. Reddy. *Theory and Analysis of Elastic Plates and Shells*. CRC Press, 2nd edition, 2006.
- [72] S.P. Timoshenko and J.M. Gere. *Theory of Elastic Stability*. Dover Publications, 2012.
- [73] J.D. Aristizabal-Ochoa. Second-order slope–deflection equations for imperfect beam-column structures with semi-rigid connections. *Engineering structures*, 32(8):2440–2454, 2010.
- [74] J. Helleland. Mechanics and effective lengths of columns with positive and negative end restraints. *Engineering structures*, 29(12):3464–3474, 2007.
- [75] I. Poutiainen, P. Tanskanen, and G. Marquis. Finite element methods for structural hot spot stress determination—a comparison of procedures. *International Journal of Fatigue*, 26(11):1147–1157, 2004.
- [76] P. Dong. A structural stress definition and numerical implementation for fatigue analysis of welded joints. *International journal of fatigue*, 23(10):865–876, 2001.
- [77] EU RAMSSES project - Lightweight high tensile steel in cruise ships. <https://www.ramsses-project.eu/solutions/steel-decks/overview/> (accessed Feb. 14, 2024).
- [78] IACS. No.47 Shipbuilding and Repair Quality Standard. https://maritimeexpert.files.wordpress.com/2018/01/rec_47_quality-standard.pdf193. pdf, 2012.
- [79] W. Shen, Y. Qiu, X. Li, X. Han, F. Berto, and D. Hu. Stress magnification effect of initial deformation on the notch stress field and fatigue strength of thin plate welded joints. *Marine Structures*, 78:102999, 2021.

- [80] J. Sandgren. Structural stress assessment for buttwelded thin plates - application and experimental validation of an analytical formulation, 2023. Aalto University, School of Engineering.
- [81] D.G. Georgiadis and M.S. Samuelides. Stochastic geometric imperfections of plate elements and their impact on the probabilistic ultimate strength assessment of plates and hull-girders. *Marine Structures*, 76:102920, 2021.
- [82] A. Tatsumi and Y. Kageyama. Ultimate strength assessment of rectangular plates subjected to in-plane compression using a statistical model of welding initial deflection. *Marine Structures*, 93:103523, 2024.
- [83] B Barsotti and M Gaiotti. Fem numerical strategies for the evaluation of the accumulated plastic strain due to a cyclic load condition. In *Advances in the Analysis and Design of Marine Structures*. CRC Press, 2023.
- [84] J. Romanoff, H. Remes, G. Socha, M. Jutila, and P. Varsta. The stiffness of laser stake welded t-joints in web-core sandwich structures. *Thin-Walled Structures*, 45(4):453–462, 2007.
- [85] J. Jelovica, J. Romanoff, S. Ehlers, and P. Varsta. Influence of weld stiffness on buckling strength of laser-welded web-core sandwich plates. *Journal of Constructional Steel Research*, 77:12–18, 2012.
- [86] L. Brubak and J. Hellesland. Computational postbuckling and strength analysis of arbitrarily stiffened plates in local and global bending. 2006.
- [87] B. Wang, S.J. Hu, L. Sun, and T. Freiheit. Intelligent welding system technologies: State-of-the-art review and perspectives. *Journal of Manufacturing Systems*, 56:373–391, 2020.
- [88] D.D. Symons and N.A. Fleck. The Imperfection Sensitivity of Isotropic Two-Dimensional Elastic Lattices. *Journal of Applied Mechanics*, 75(5):051011, 07 2008.
- [89] M.F. Zaeh and G. Branner. Investigations on residual stresses and deformations in selective laser melting. *Production Engineering*, 4:35–45, 2010.
- [90] R.N. Glaesener, S. Kumar, C. Lestringant, T. Butruille, C.M. Portela, and D.M. Kochmann. Predicting the influence of geometric imperfections on the mechanical response of 2d and 3d periodic trusses. *Acta Materialia*, 254:118918, 2023.
- [91] A. Rossi, A.S. Clemente de Souza, R. Silva Nicoletti, and C.H. Martins. The influence of structural and geometric imperfections on the ldb strength of steel–concrete composite beams. *Thin-Walled Structures*, 162:107542, 2021.
- [92] M.P. Alves, C.A. Cimini Junior, and S.K. Ha. Fiber waviness and its effect on the mechanical performance of fiber reinforced polymer composites: An enhanced review. *Composites Part A: Applied Science and Manufacturing*, 149:106526, 2021.

Errata

Publication I

The centre line distortion of panel P1.2 in the demo-block configuration is incorrect in Fig. 6. Please, consider the profile shown in Fig. 9 in PII.

In the field of cruise shipbuilding, the desire for better efficiency and sustainability has promoted the integration of lightweight solutions, among which the employment of thin plates in welded superstructure decks offers promising advantages. Nonetheless, a more pronounced susceptibility to irregular welding-induced distortions has been observed on thin plates. Extensive research has revealed the need for full-field scanning and subsequent numerical modelling of the distorted plates to ensure accurate structural assessment. However, this comes at a cost, both in terms of resources and time. As a contribution to the development of thin-walled, large, welded structures, this thesis investigates on more efficient structural stress assessment approaches for 4-mm butt-welded thin plates in ship-deck panels.



ISBN 978-952-64-1868-1 (printed)

ISBN 978-952-64-1869-8 (pdf)

ISSN 1799-4934 (printed)

ISSN 1799-4942 (pdf)

Aalto University
School of Engineering
Department of Mechanical Engineering
www.aalto.fi

**BUSINESS +
ECONOMY**

**ART +
DESIGN +
ARCHITECTURE**

**SCIENCE +
TECHNOLOGY**

CROSSOVER

**DOCTORAL
THESES**